

RESEARCH ARTICLE

10.1002/2014JD022925

Key Points:

- A strong Arctic cyclone is well reproduced using an ensemble reanalysis
- Additional Arctic radiosondes improve the prediction of an Arctic cyclone
- Cyclogenesis depends on the presence of a tropopause polar vortex

Correspondence to:

A. Yamazaki,
yzaki@jamstec.go.jp

Citation:

Yamazaki, A., J. Inoue, K. Dethloff, M. Maturilli, and G. König-Langlo (2015), Impact of radiosonde observations on forecasting summertime Arctic cyclone formation, *J. Geophys. Res. Atmos.*, 120, doi:10.1002/2014JD022925.

Received 2 DEC 2014

Accepted 24 MAR 2015

Accepted article online 26 MAR 2015

Impact of radiosonde observations on forecasting summertime Arctic cyclone formation

Akira Yamazaki¹, Jun Inoue^{2,3}, Klaus Dethloff⁴, Marion Maturilli⁴, and Gert König-Langlo⁵

¹Application Laboratory, Japan Agency for Marine-Earth Science and Technology, Yokohama, Japan, ²Institute of Arctic Climate and Environment Research, Japan Agency for Marine-Earth Science and Technology, Yokosuka, Japan, ³National Institute of Polar Research, Tokyo, Japan, ⁴Helmholtz Centre for Polar and Marine Research, Alfred Wegener Institute, Potsdam, Germany, ⁵Helmholtz Centre for Polar and Marine Research, Alfred Wegener Institute, Bremerhaven, Germany

Abstract The impact of Arctic radiosonde observations on the forecasting of the 2012 early August Arctic cyclone AC12—the “strongest” since records began—has been investigated using an observing system experiment (OSE). An atmospheric ensemble reanalysis (ALERA2) was used as the control experiment (CTL) to reproduce the development of the Arctic cyclone and surrounding large-scale atmospheric fields. The OSE applies the same reanalysis as the CTL except for the exclusion of radiosonde observations from the German icebreaker *Polarstern*, which cruised near Svalbard during mid-July to early August 2012. Comparison of the two reanalyses revealed a difference in the upper tropospheric circulation over northern mid-Eurasia, just before the Arctic cyclone developed, in the form of a stronger tropopause polar vortex in the CTL. This indicated that the upper tropospheric field in the CTL had greater potential for baroclinic instability over mid-Eurasia. Ensemble predictions were then conducted using the two reanalyses as initial values at which the tropopause polar vortex approached northern mid-Eurasia. The CTL prediction reproduced the formation of the Arctic cyclone, but the OSE shows a significantly weaker one. These results indicate that the improved reproduction of upper tropospheric circulation in the Arctic region due to additional radiosonde observations from a mobile platform was indispensable for the prediction of AC12. In particular, observations being acquired far from the Arctic cyclone affect the prediction of the cyclone via the upper tropospheric circulation in the atmospheric west wind drift.

1. Introduction

On the broad scale, the atmosphere in the northern polar cap region can be considered as a massive low-pressure system. This low corresponds to a colder tropospheric air mass relative to the tropical and midlatitude regions, which affects midlatitude weather whenever it seeps out to lower latitudes [e.g., Mori et al., 2014; Shoji et al., 2014]. In terms of large-scale atmospheric dynamics, the variability of this low is sometimes interpreted as the Arctic Oscillation (AO) [Thompson and Wallace, 1998] and/or North Atlantic Oscillation (NAO) [Ambaum et al., 2001]. The AO/NAO exists in all seasons and even though its amplitude becomes smaller in summer relative to winter [Barnston and Livezey, 1987; Thompson and Wallace, 2000], its variability and influence on various atmospheric phenomena can be said to exist perennially. Therefore, an understanding of the dynamics of the low is important in explaining various weather and climate patterns.

The massive low is composed of inherent, multiscale cyclones of the order 100–10,000 km rather than a single coherent structure. Of the inherent cyclones, two types are worthy of particular attention: the tropopause polar vortex (TPV) [Cavallo and Hakim, 2009, 2010, 2012] and the Arctic cyclone [Tanaka et al., 2012]. Because both types have large amplitude with a radius of 500–1000 km and are long-lived features that persist for more than ~10 days, they exert considerable influence on weather and climatic patterns.

TPVs are cyclones at the tropopause in the Arctic region that are characterized by relatively high potential vorticity or low potential temperature. They occur frequently along Arctic coastal regions, especially along the northwestern coast of Greenland and along the coast of northern Siberia [Cavallo and Hakim, 2009]. For example, a TPV sometimes appears in a westerly jet as a trough, affecting midlatitude weather by meandering in the westerly jet and/or modifying the baroclinicity [e.g., Bosart et al., 1996], which consequently affects surface cyclones.

Arctic cyclones appear at sea level over the Arctic Ocean, originating over the Arctic Ocean or subtropical oceans (North Atlantic and Pacific) or continents (Eurasia or North America). Similar to TPVs, some Arctic

cyclones persist for more than 10 days [Simmonds and Rudeva, 2012; Tanaka et al., 2012], which is considerably longer than the lifetime of surface cyclones in other latitudes. Such persistence implies that Arctic cyclones have unique dynamical properties; however, their mechanisms and dynamics have received little attention. A small number of investigations have stemmed from sparse data observed over the Arctic Ocean. However, the focus on Arctic climate change has partly led to more intensive observations, which together with significant developments regarding reanalysis data, will enable investigations into the mechanisms of Arctic cyclones [Tanaka et al., 2012; Aizawa et al., 2014].

Zhang et al. [2004] investigated the seasonal climatology of Arctic cyclones. Arctic cyclones occur in all seasons and the number of cyclones is almost the same in summer and winter; however, locally, the number of cyclones originating from the North Pacific, Eurasia, and North America in summertime is larger. They also found that the intensities and durations of Arctic cyclones in summer are generally stronger than in winter. More recently, Simmonds et al. [2008] investigated the climatology and trends of Arctic cyclones by applying their cyclone-tracking method to three reanalysis data sets. Although they found that the total number of cyclones in winter is larger than that in summer, summer Arctic cyclones are still numerous and very active over the Arctic Ocean. These results imply that summertime cyclone activity has greater impact on the climate and weather of the Arctic region, and therefore, they are worthy of investigation.

The summertime climate and weather in the Arctic have received increasing attention because of their influence on Arctic sea ice reduction in summer and vice versa. The Arctic region has been experiencing rapid warming and changes of the climatic fields in the region have caused a retreat of sea ice. Therefore, the mechanism of how atmospheric pressure systems interact with sea ice is important. Previous studies have shown that reduction in sea ice is linked to climatic changes, not only in the Arctic but also in midlatitude regions via changed large-scale atmospheric circulations [Honda et al., 2009; Inoue et al., 2012; Rinke et al., 2013; Cohen et al., 2014; Mori et al., 2014; Vihma, 2014]. Nonetheless, there remain many ambiguities regarding the mechanism, which numerous studies have recently attempted to clarify [Screen and Simmonds, 2013; Screen et al., 2013; Screen et al., 2014; Sato et al., 2014; Simmonds and Govekar, 2014]. From a local viewpoint, consideration of the impacts of synoptic-scale atmospheric phenomena has been focused on sea ice reduction on seasonal scales [Simmonds and Rudeva, 2012; Zhang et al., 2013], and even on sea ice variations on synoptic scales. One of the most important synoptic-scale phenomena is the Arctic cyclones because they are more intense and have longer durations. Therefore, the behavior and predictability of these cyclones should be investigated rigorously.

As a first step, the mechanism of formation of Arctic cyclones would be worth investigating because this is related directly to their numbers and climatology. Although some unique mechanisms have been proposed for the formation of Arctic cyclones [e.g., Tanaka et al., 2012; Aizawa et al., 2014], an orthodox mechanism for the formation of extratropical cyclones, namely baroclinic instability in a baroclinic zone, can be adopted for their formation [Simmonds and Rudeva, 2012]. Such a baroclinic zone is formed in summer over Eurasia owing to the land-sea contrast, making this one of the main regions for Arctic cyclone genesis [Serreze and Barrett, 2008]. However, studies on the formation of Arctic cyclones, especially in summer, are limited in comparison to other extratropical or tropical cyclones. Therefore, in this work, a descriptive and predictive study of the formation of summer Arctic cyclones was conducted through a case study of a most intense one, using data analyses and forecasting experiments.

The investigated case focuses on the Arctic cyclone AC12, which occurred in early August 2012. AC12 is given the adjective "great" because its surface central pressure was the lowest of any Arctic cyclone during August since records began in 1979 [Simmonds and Rudeva, 2012; Nishii et al., 2015]. During August 2012, the extent of the Arctic sea ice plummeted to new record low, such that its relationship with the cyclone is also a subject of interest [Zhang et al., 2013; Simmonds, 2015]. Regarding the formation and development mechanisms of Arctic cyclones, Simmonds and Rudeva [2012] suggested the importance of an upper level trough or TPV to the intense deepening of the surface cyclone, i.e., AC12. In other words, the surface features of AC12 would be developed by mutual interaction with the TPV via baroclinic instability. To quantify the significance of the TPV in the formation and development of AC12, a comparison of atmospheric circulations in which the reproduction of the TPV differs would be useful. Reproduction of atmospheric fields can be controlled by using our developed data assimilation system (introduced in section 2.1) and by conducting an observing system experiment (OSE), which is a

reanalysis generated by a data assimilation system within which specific observations are added or excluded. Here reproducibility is defined as the impact that specified observations have on resolving a feature in reanalysis data. Reproducibility is calculated as the difference between the CTL and OSE (CTL – OSE).

In a related study using an OSE, *Inoue et al.* [2013] reported that additional radiosonde data over the Arctic region in the fall 2010 had a considerable impact on reproducibility of the upper level circulation. They suggested that the use of observational data nearby of an Arctic cyclone [*Inoue and Hori*, 2011], obtained by the Japanese research vessel *Mirai*, exerted an influence on the reproducibility of the entire Arctic and midlatitude atmospheric circulations via the upper troposphere. They revealed the importance of additional radiosonde observations in the Arctic region to the reproducibility of large-scale atmospheric circulations; however, the impact on synoptic-scale disturbances remains unknown. Hence, comparisons of upper tropospheric circulation fields with differing reproduction, obtained by an OSE, could clarify the contribution of the TPV to the AC12 disturbance. Motivated by the earlier studies listed above, we examined the impact of extra radiosonde observations over the Arctic region on the forecast of one of the most extreme disturbances, AC12.

In this study, twice-daily radiosonde observations performed by the German research vessel *Polarstern* from mid-July to August of 2012 near Spitsbergen Island (Svalbard) were used. In mid-July, the TPV that influenced the development of AC12 was located over Svalbard [*Simmonds and Rudeva*, 2012]; hence, additional observations could influence the reproducibility and prediction of the cyclone's development. It should be mentioned that the locations of the observations were far upstream from the position of AC12 at its mature stage (Figure 1); therefore, the impact of the observations, if any, must have had a remote effect on the development of the cyclone.

To conduct the OSE and quantify their impact, the *Polarstern* radiosonde data were excluded from an ensemble data assimilation system called ALEDAS2 [*Enomoto et al.*, 2013], which is composed of the Atmospheric GCM for the Earth Simulator (AFES) [*Ohfuchi et al.*, 2004; *Enomoto et al.*, 2008; *Kuwano-Yoshida et al.*, 2010] and the local ensemble transform Kalman filter (LETKF) [*Hunt et al.*, 2007; *Miyoshi and Yamane*, 2007]. Reanalysis data sets generated by the system excluded the *Polarstern* radiosonde data and were used as the OSE reanalysis and by ALEDAS2 as the control (CTL) in data analyses and ensemble forecast experiments. These experiments are described in the following section.

2. Data and Methods

2.1. Ensemble Reanalysis: ALERA2

First, we observe the temporal evolution of AC12 via realistic reanalysis data. As the reference reanalysis (CTL), the AFES-LETKF experimental ensemble reanalysis version 2 (ALERA2) data set produced with ALEDAS2 was used. The ALERA2 data set encompasses the period from January 2008 to December 2012 and thus includes the period for which AC12 occurred. ALEDAS2 comprises AFES for forecasts and LETKF for analyses. In the forecast step of ALEDAS2, an ensemble forecast is conducted with AFES of which a horizontal resolution is T119 (triangular truncation with truncation wave number of 119, $1^\circ \times 1^\circ$) and vertical levels are L48 (σ -level, up to about 3 hPa). The horizontal resolution of AFES is relatively modest for Arctic cyclones, although higher-resolution reanalysis systems would of course better represent the cyclones [*Tilinina et al.*, 2014]. The sea surface temperature and the sea ice thickness were prepared from the National Oceanic and Atmospheric Administration daily $1/4^\circ$ OISST (optimal interpolation sea surface temperature) version 2 [*Reynolds et al.*, 2007]. In the analysis step, observations are assimilated into the ensemble forecast with LETKF; observations were prepared from PREPBUFR data sets compiled by the National Centers for Environmental Prediction (NCEP) and archived at the University Corporation for Atmospheric Research (UCAR). The summary of the configuration of ALEDAS2 is presented in Table 1. Note that the CTL is the same reference reanalysis as used in *Inoue et al.* [2013]. Further details regarding ALERA2 and ALEDAS2 are described by *Enomoto et al.* [2013]. In the following, it is found that the CTL (ALERA2) can reproduce the time evolution of AC12 and the surrounding large-scale circulation fields. Large-scale (environmental) and synoptic fields of AC12 formation in the CTL are examined via data analyses in section 3.

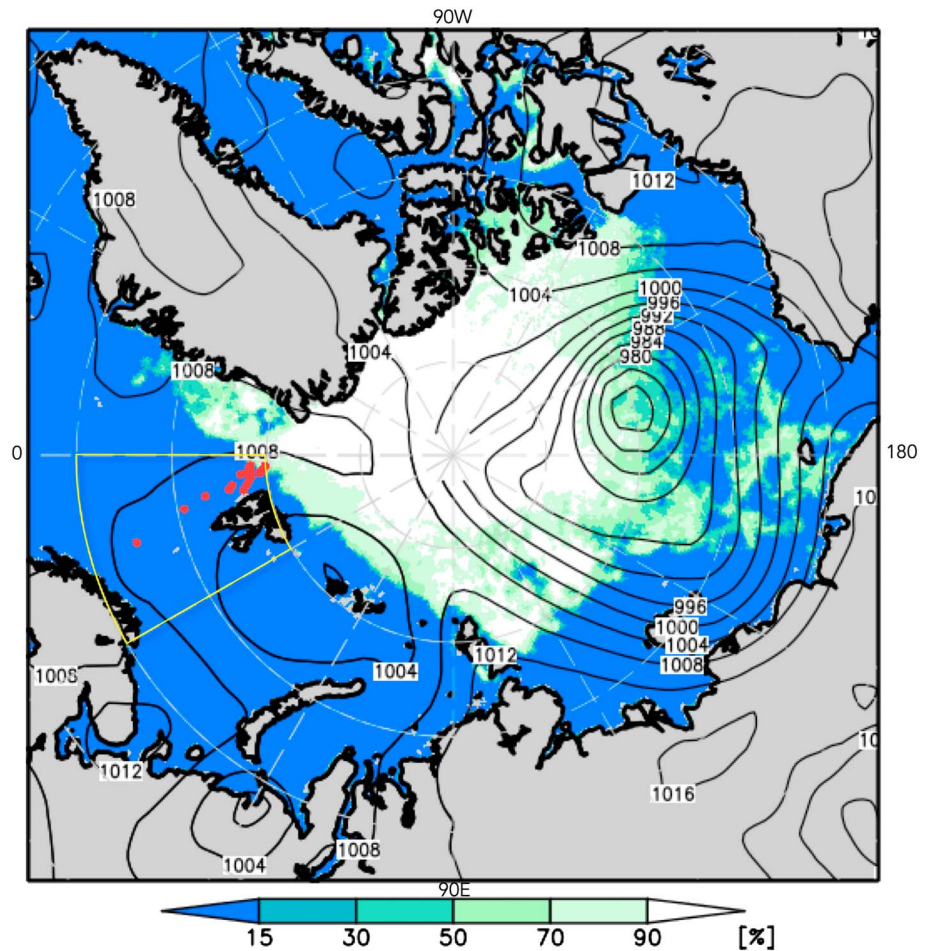


Figure 1. Locations of radiosonde observations performed by the *Polarstern* (red dots) during 13–29 July 2012, sea level pressure at 00:00 UTC on 6 August 2012, in ERA-Interim (ERA-I), and sea ice concentration on 6 August 2012, in AMSR2. Area defined by yellow line near Svalbard indicates the averaging region used for Figure 11.

An advantage of using ALERA2 is that it enables OSE, through which the impacts of specific observations can be quantified and thus the reproducibility of atmospheric fields controlled. The specific observations used for AC12 were the *Polarstern* radiosondes detailed in section 4. Details of the OSE for AC12 are also in section 4.

2.2. Forecast Experiments

Forecast experiments of AC12 formation are conducted following the data analysis, to examine our hypothesis that TPV reproducibility is important in forecasting AC12. The forecast model (AFES) is the same model used in ALEDAS2, which is also used to create ALERA2 (Table 1). Therefore, the forecast results can be compared with the CTL. Also, ensemble forecasting provides uncertainty.

As initial values in the experiments, ALERA2 (CTL or OSE) are used. That is, the forecast experiments use the framework of ALEDAS2 execution without data assimilation. The reanalysis OSE in which the *Polarstern* radiosonde observations were not assimilated were also used as initial values. We compare forecast results from the CTL with those from the OSE and can therefore estimate the impact of the radiosonde observations on the AC12 forecast. Results of the forecast experiments are described in section 5.

3. Large-Scale and Synoptic Fields in ALERA2

We first checked whether the CTL could reproduce “real” atmospheric fields. Based on *Simmonds and Rudeva* [2012], who highlighted the importance of the TPV for the surface development of AC12, we verified the reproduction of the large-scale and synoptic fields in the CTL at both the tropopause and the surface. Note

Table 1. Configuration of ALEDAS2 for Reanalysis Data Set ALERA2 and Ensemble/Deterministic Prediction System (EPS/DPS) for Forecast Experiments

ALEDAS2			
Atmospheric GCM	AFES		
Dynamical core	Spectral, Eulerian, and primitive equation		
Horizontal resolution	T119 (~1° × 1°)		
Vertical levels	L48 (σ level, up to about 3 hPa)		
Boundary conditions	OISST daily 1/4°		
Data assimilation method	LETKF		
Ensemble size	63		
Observations	NCEP PREPBUFR		
Data assimilation window	6 h		
Ensemble Prediction System (EPS) and Deterministic Prediction System (DPS)			
	EPS	DPS	
AGCM		AFES (T119L48)	
Boundary conditions		OISST daily 1/4°	
Ensemble size	63		1
Initial condition	ALERA2		ERA Interim
Start date		00 UTC 3 August 2012	
Length of forecasts		5 days	

that *Simmonds and Rudeva* [2014] further revealed that TPVs were involved with almost all of 60 intense Arctic cyclones. The large-scale fields were compared with ERA Interim (ERA-I) [Dee et al., 2011] data in both the upper and lower troposphere. Figure 2 shows the 10 day averaged upper level geopotential height and sea level pressure (SLP) fields in CTL and ERA-I. It can be seen that the circulation fields in CTL correspond well with those in ERA-I. Although SLP in the CTL near the pole shows weaker amplitude than in the ERA-I (Figures 2c and 2d), it reflects the underestimation of the amplitude of AC12 in the CTL, rather than a difference in the environmental field of AC12. This could be caused by the shortage of satellite observations in the NCEP PREPBUFR assimilated in the CTL and the resolution of the GCM used for ALEDAS2: The resolution of ERA-I is T255L60 [Dee et al., 2011], which is horizontally more than twice that of ALEDAS2. However, the atmospheric pattern in the CTL is generally reproduced as well as in the ERA-I. Tracks of the centers of AC12 and the TPV are also shown in Figure 2. The centers are detected by minimum points of SLP and 300 hPa geopotential height (Z300) at each time interval in the prescribed region (60°N–90°N, 90°E–120°W). Note that the centers of the TPV and the surface cyclone generally move from west to east. Overall, the tracks of the TPV and AC12 are similar in both the CTL and the ERA-I. AC12 develops from two different surface cyclones that later merge during this time period. The first surface cyclone, over the Arctic Ocean, moves from west to east during 2–4 August, corresponding to the northern course. The second surface cyclone emerges over mid-Eurasia on 3 or 4 August and moves toward the northeast and then the north, corresponding to the southern course. The first cyclone merges with and is absorbed by the second on 5 August 2012. With regard to the discussion on the formation of AC12, it is considered not essentially problematic that the northern course in the CTL is somewhat different to that in the ERA-I, because the first cyclone is absorbed and thus is subordinate to the second surface cyclone that is AC12. These processes are explained further in the description of the synoptic field. Therefore, it is concluded that CTL reproduces the environmental fields of AC12 satisfactorily. Therefore, CTL is treated as a reanalysis representative of the real atmosphere.

In the following, the time evolutions of AC12 and the TPV are described as synoptic fields. The developing and mature stages of AC12 with the TPV are then considered in Figure 3. The two stages are separated as follows: The developing stage is considered as the period from 1 to 4 August and the mature stage as 5–9 August. In the developing stage, the surface cyclone of AC12 formed over mid-Eurasia near the Laptev Sea at around 12:00 UTC on 3 August and then moved to northern East Siberia. At this time, two surface cyclones existed: AC12 over the Eurasian continent and another preexisting cyclone over the Arctic Ocean. It can be seen that AC12 displays a west-tilted structure with an upper tropospheric trough, which is typical of baroclinic instability, and thus, its amplitude increased. The upper tropospheric trough is the TPV

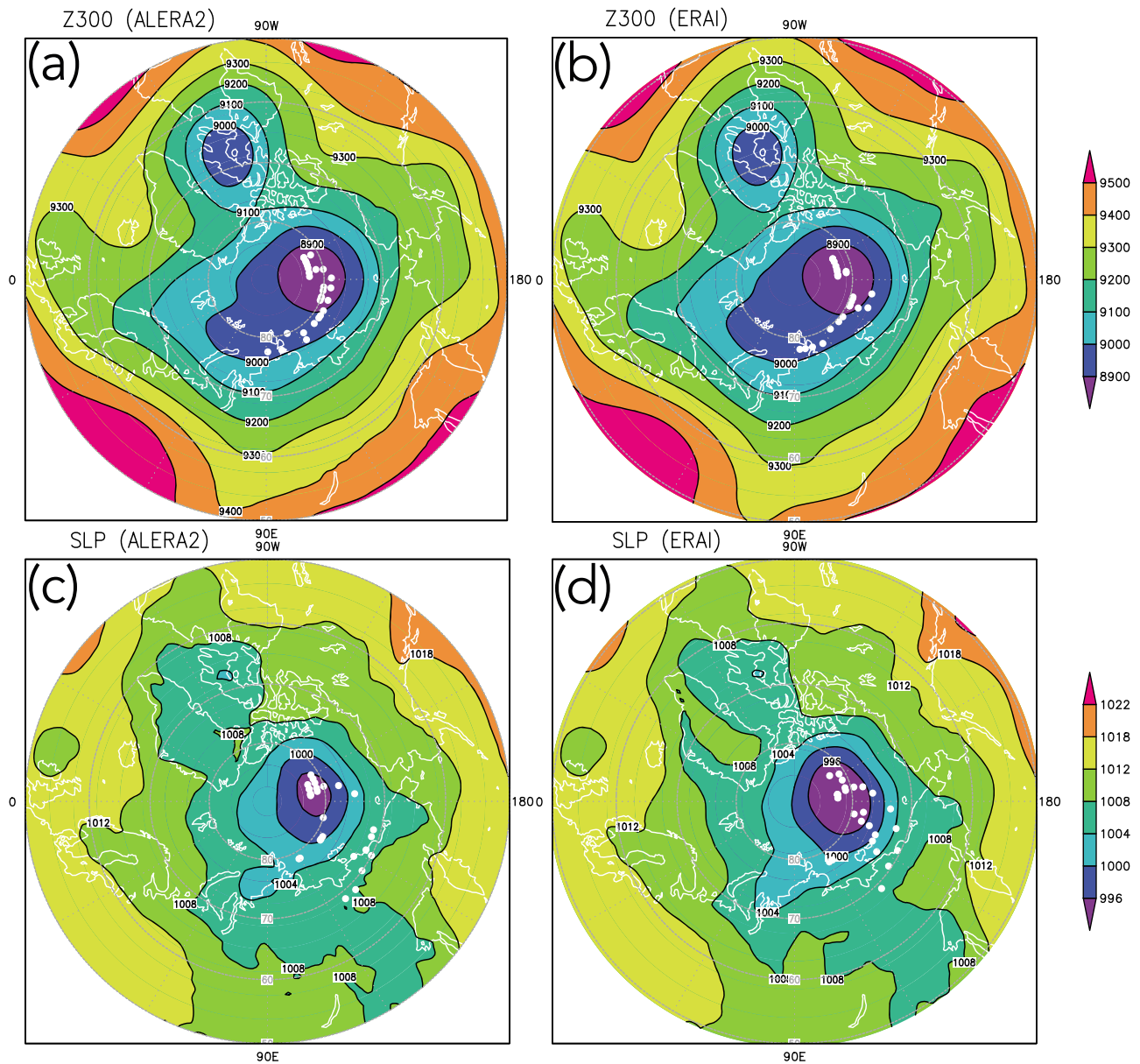


Figure 2. Time-averaged (a and b) 300 hPa geopotential height (Z300; m) and (c and d) sea level pressure (SLP; hPa) during 1–10 August 2012, in the ALERA2 ensemble means (CTL) and ERAI. White dots indicate the centers of the surface cyclone (AC12) and TPV between 00:00 UTC 2 August and 18:00 UTC 9 August at 6-hourly intervals. See text for more details.

originating upstream at Svalbard [Simmonds and Rudeva, 2012]. AC12 then absorbed the other surface cyclone and in the mature stage, and the cyclone’s structure became equivalent barotropic with the TPV as it traversed the Arctic Ocean: This is indicative of the vertical vortex coupling mechanism proposed by Aizawa *et al.* [2014] and Simmonds and Rudeva [2014], which can lead to rapid intensification of Arctic cyclones. However, clarifying this mechanism is beyond the scope of this paper, since we focus on the formation of AC12 prior to the rapid intensification. AC12 has its minimum SLP during the equivalent barotropic phase of its lifecycle, which is a characteristic similar to that of the mature extratropical cyclone structure reported by Čampa and Wernli [2012]. The SLP minimum of AC12 might be accomplished by the superposition of the TPV and the surface cyclone.

Time sequences of the vertical (potential) temperature distribution of AC12 are shown in Figure 4. We see that the vertical distribution is substantially different between the developing and mature stages. In the former stage (before 5 August) when AC12 traversed the Eurasian continent, it did not have the upper tropospheric

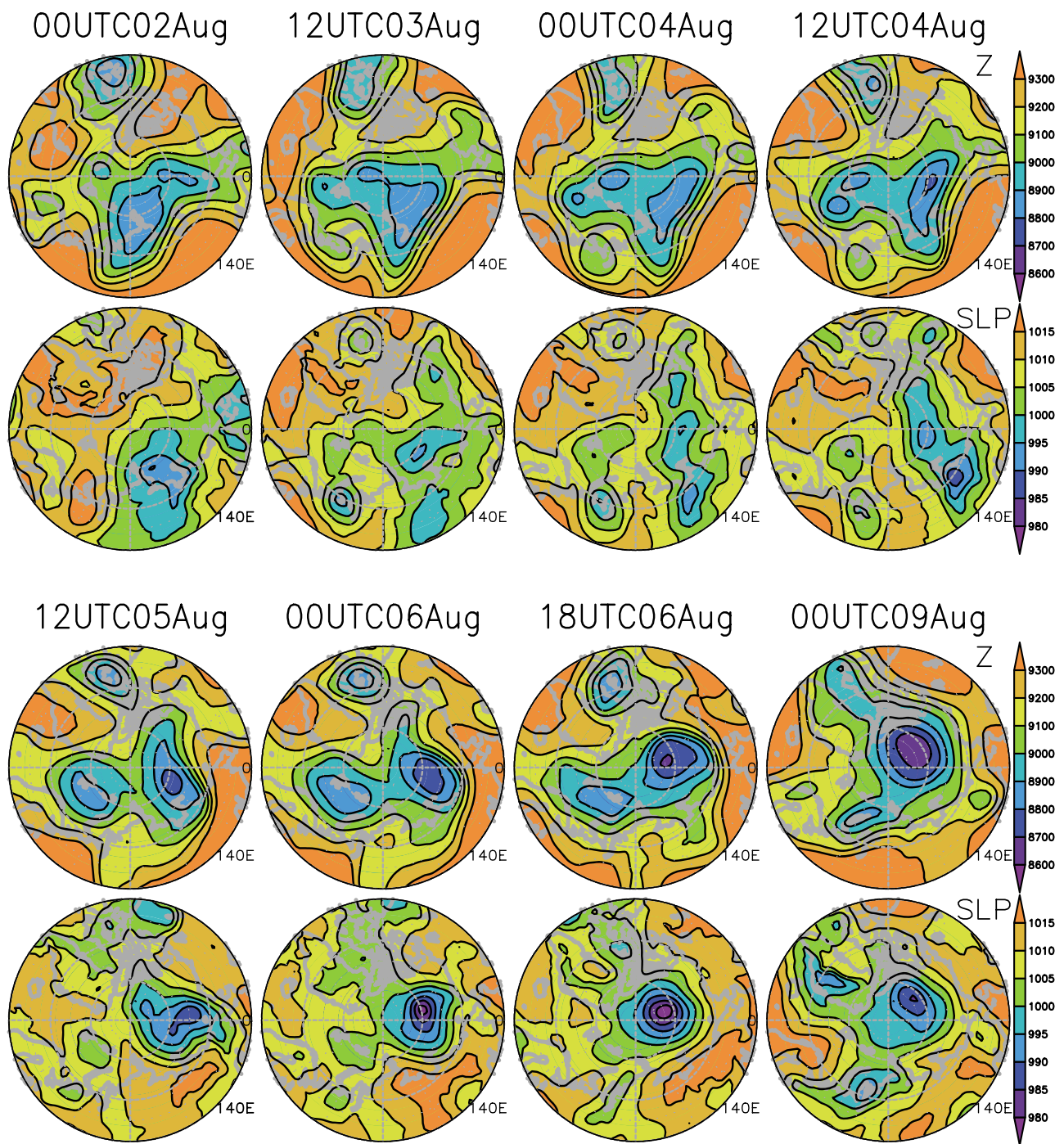


Figure 3. Time evolutions of AC12 and the TPV in the (top) developing and (bottom) mature stages for Z300 (m) and SLP (hPa) in CTL.

warm core corresponding to the descending region of lower stratospheric air due to a tropopause folding, i.e., the TPV. This indicates that the TPV departed from the AC12 surface cyclone locations; AC12 and the TPV formed a baroclinic structure. In the mature stage (after 5 August) when AC12 was over the Arctic Ocean, it had the upper tropospheric warm core, so it became vertically coherent and equivalent barotropic with the TPV. AC12 also had a lower tropospheric cold core during this stage, implying strong static stability near the tropopause; i.e., there was high potential vorticity air corresponding to the TPV in the upper troposphere [Tanaka et al., 2012; Aizawa et al., 2014].

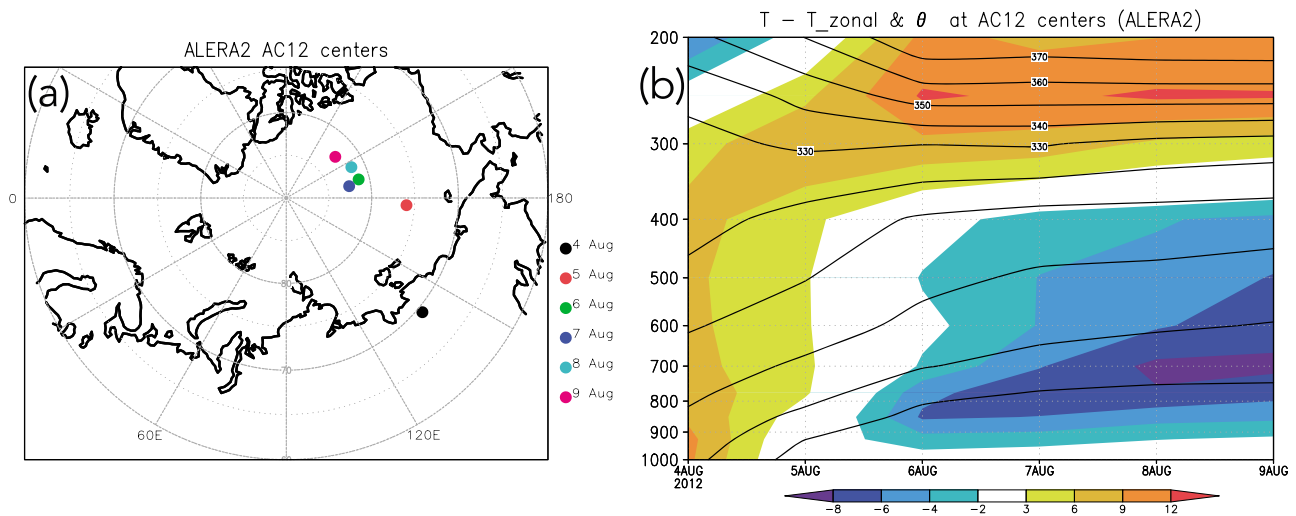


Figure 4. (a) Daily positions of AC12 centers as dots and (b) temporal evolution of daily vertical temperature distribution at the centers. Dot colors in Figure 4a indicate dates as in legend. Shades and contours in Figure 4b show temperature anomalies from zonal averages (K) and potential temperature (θ ; K) at the centers, respectively.

Through the two stages, we focus on the baroclinic growth of AC12 over the Eurasian continent during the developing stage, i.e., the formation of AC12. Because baroclinic instability requires an upper tropospheric trough, the TPV that acts as the trough is essential for the formation of AC12. A PV- θ view (where PV and θ are potential vorticity and potential temperature, respectively) [Hoskins, 1991] is introduced to investigate the baroclinic growth (Figures 5 and 6). In the beginning, the vertical layer of the tropopause is specified. In a large-scale vertical distribution of Ertel PV and θ (Figure 5), we see that the location of the (dynamical) tropopause between 13 July and 9 August is at 2 PVU (potential vorticity unit), 320 K, or 300 hPa. This is because above this PV surface, vertical gradients of PV or θ are dense, so the TPV is on this PV surface.

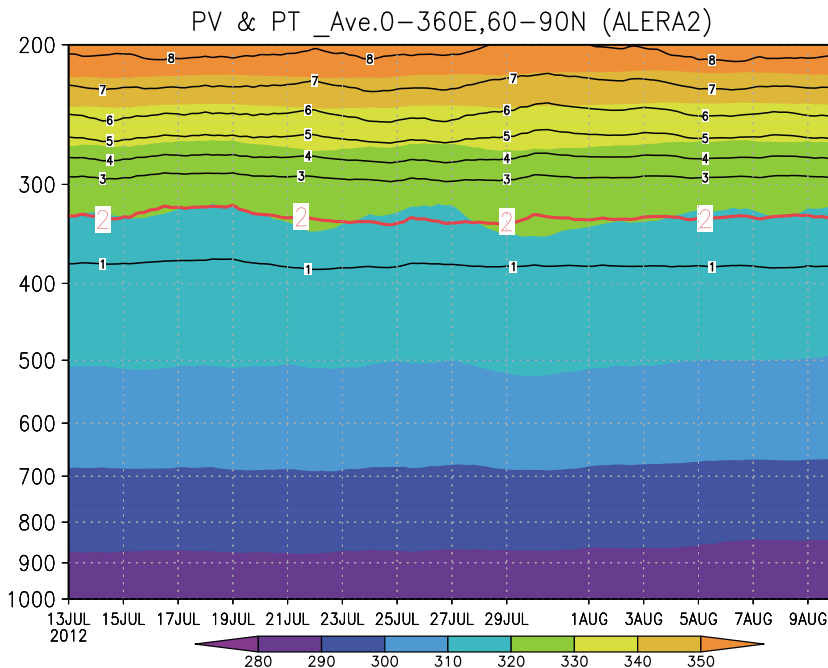


Figure 5. Pressure-time cross section of potential vorticity (PV, contours; PVU) and θ (shading; K) averaged to the north of 60°N.

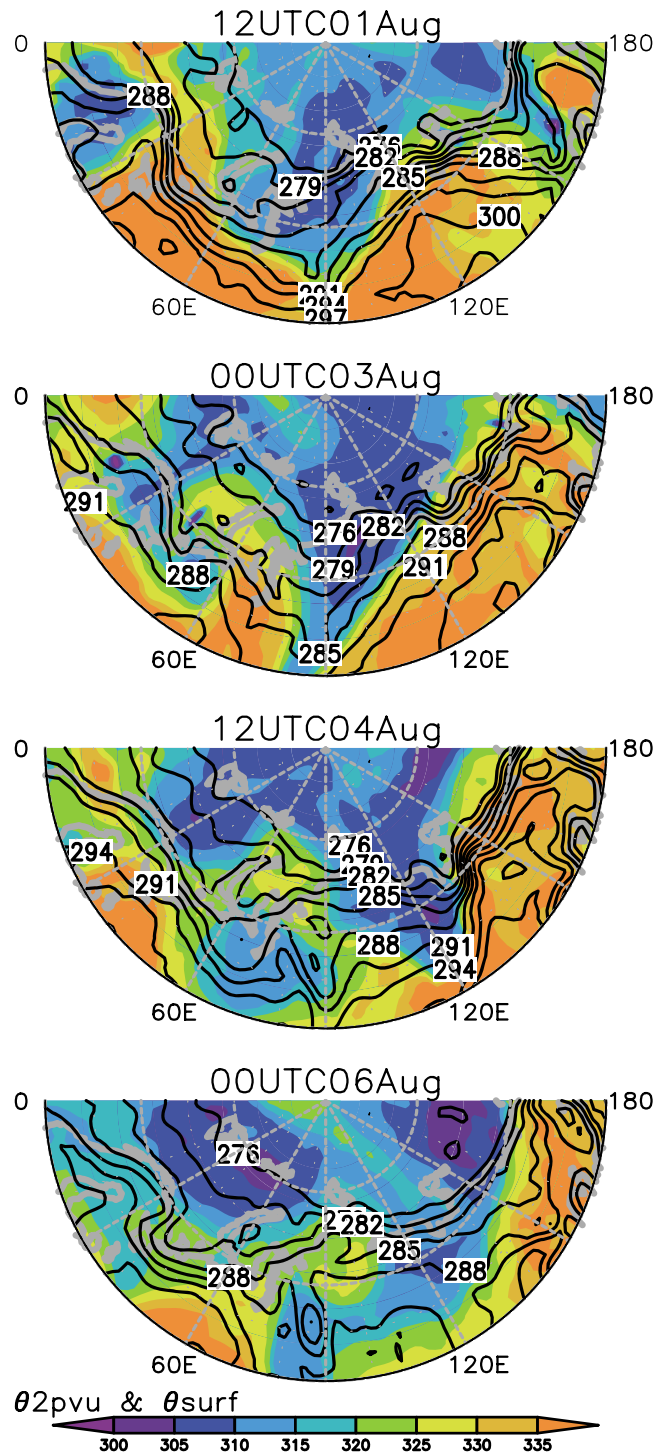


Figure 6. Snapshots of θ at 2 PVU (θ_{dt} , shading; K) and surface θ (contours; K) in developing and mature stages of AC12.

impact of the radiosonde observations on TPV reproduction, i.e., we controlled that reproducibility. Afterward, we examine the importance of the TPV in forecasting AC12.

4.1. Radiosonde Observations by R/V *Polarstern*

The *Polarstern* conducted cruises near Svalbard from 13 to 29 July 2012 (ARK-XXVII/1 and ARK-XXVII/2) and over the Arctic Ocean from 2 August to 8 October 2012 (ARK-XXVII/3). During the cruises, GPS radiosonde

Temporal evolution of the dynamical tropopause (2 PVU surface) θ_{dt} and surface θ are displayed (Figure 6). In the developing stage, surface θ in Eurasia shows a strong meridional gradient in a baroclinic band due to the thermal contrast between the warm Eurasian continent and cold Arctic Ocean [Serreze *et al.*, 2001]. Just before the surface cyclone starts to develop (about 3 August), a low θ_{dt} trough at the tropopause, which is the TPV near the Kara Sea, elongates southward from the large-scale low- θ_{dt} air extending zonally across the north polar cap region and touches the baroclinic zone. Subsequently, the surface cyclone begins to develop and move northeast along the band, together with the TPV.

Thus, the circulation of the upper troposphere in the polar region substantially contributes to the development of AC12 at the surface. In turn, it is suggested that the reproducibility of the TPV, originating from the large-scale, low- θ_{dt} air that is connected directly with the Svalbard region and observed by the *Polarstern*, can affect the prediction of the formation of the AC12.

4. Observing System Experiment (OSE)

Inoue *et al.* [2013] showed through their OSE study that additional radiosonde observations in the Arctic region during fall 2010 altered upper troposphere reproduction there. This finding implies that such additional observations during AC12 could improve TPV reproduction, which would be important in the formation of AC12. Additional observations were made by the *Polarstern* during July and August 2012 in the Arctic region.

We therefore conducted an OSE similar to Inoue *et al.* [2013] and estimated the

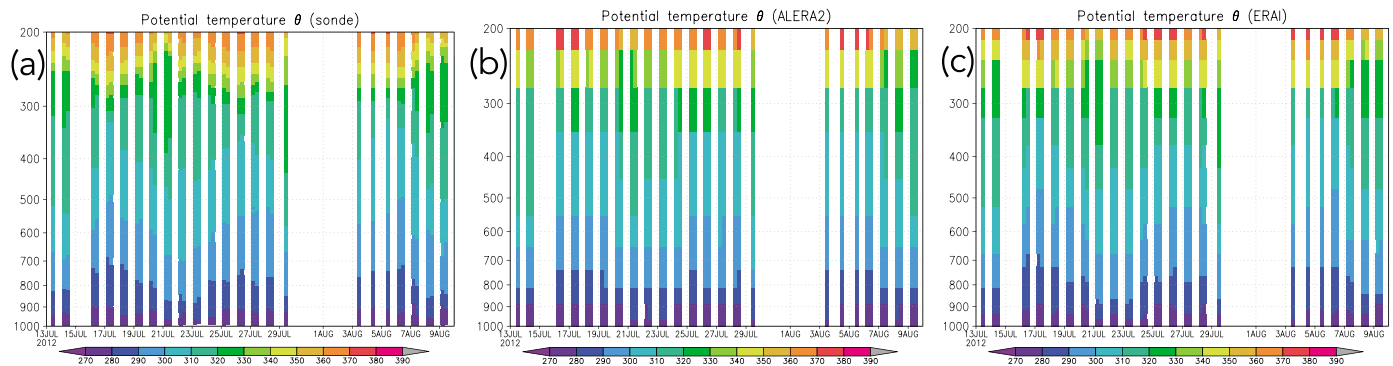


Figure 7. Vertical profiles: (a) radiosonde observations, (b) ALERA2 (CTL) analysis ensemble mean, and (c) ERAI potential temperature θ (K) at the observation locations of *Polarstern*. Vertical and horizontal axes indicate pressure (hPa) and time, respectively.

observations (Vaisala RS92-SGPW) were performed routinely twice daily at around 05:00 and 11:00 UTC [König-Langlo, 2012]. All sounding data were sent to the Global Telecommunication System, suggesting that the upper tropospheric environment is better represented by observations in the reanalysis field, e.g., ERAI. To verify the reproduction of the tropopause in the CTL at the observation points, we compared CTL with the radiosonde observations using the time-height cross section of the air temperature during the observation period at the grid point nearest to the ship positions (Figure 7). From the radiosonde data (Figure 7a), we found high θ (>320 K) near 300 hPa with some temporal variation in the vertical, which correspond to the tropopause (Figure 5). In the CTL (Figure 7b), the tropopause was reproduced at the right time. In addition, a comparison of the CTL with the ERAI (Figure 7c) showed that they had similar structures and time evolutions.

It is important to emphasize that the locations of soundings during 13–29 July (i.e., over the Fram Strait) were far from the position of the mature AC12 (Figure 1). Therefore, an evaluation of the impact of the sounding data on the reproducibility of AC12 using ALEDAS2 was considered worthwhile.

Figure 8 displays the environmental pattern for which AC12 developed in the CTL. The horizontal distribution of θ_{dt} (Figure 8a) shows a band of relatively low θ_{dt} air centered poleward of the Eurasian coast, and covering Svalbard and northern Russia. There are two important points regarding this low- θ_{dt} air. The first is that the iso- θ_{dt} areas near the observation points (Svalbard) are ventilated toward Russian coastal regions facing the area of Arctic Ocean in which AC12 developed and became most intensified. As advection moves air parcels over one of the areas in several days, the observationally adjusted fields from *Polarstern* could impact the environment around which AC12 developed. The second point is that the PV gradients near the observation points are also connected with the location of AC12 at 300 hPa (Figure 8b). Rossby waves are focused along horizontal PV gradients, which are relatively high near the tropopause, and act to propagate energy downstream along this gradient. Hence, the large-scale structure of AC12 implies that the atmospheric circulation around Svalbard remotely connected with that around the Russian coastal region where the TPV became apparent in the upper level PV and θ field.

In this study, we prepared two sets of experimental reanalyses. The first was the CTL, which assimilated sounding data from *Polarstern* as well as routine observations (NCEP PREPBUFR), and the second was the OSE, which assimilated the same observations but excluded the 39 *Polarstern* soundings (from 11:00 UTC 13 July to 11:00 UTC 29 July 2012, and from 11:00 UTC 3 August to 11:00 UTC 9 August 2012) [König-Langlo, 2012].

By comparing the CTL with OSE reanalyses, the impact of the radiosonde observations on AC12 can be investigated. The difference between the reanalysis fields is expected to be small because both assimilate the same quantity of data, except for the few *Polarstern* observations.

4.2. Comparison of the Reanalyses

A comparison of the reanalyses shows that the differences between AC12 (surface cyclone) and TPV amplitudes are in the range of ~ 1 hPa and ~ 10 m, respectively (Figure 9), which are small with respect to the deviations of synoptic time scales or zonal asymmetries. Both the CTL and OSE reproduce the time evolutions of the

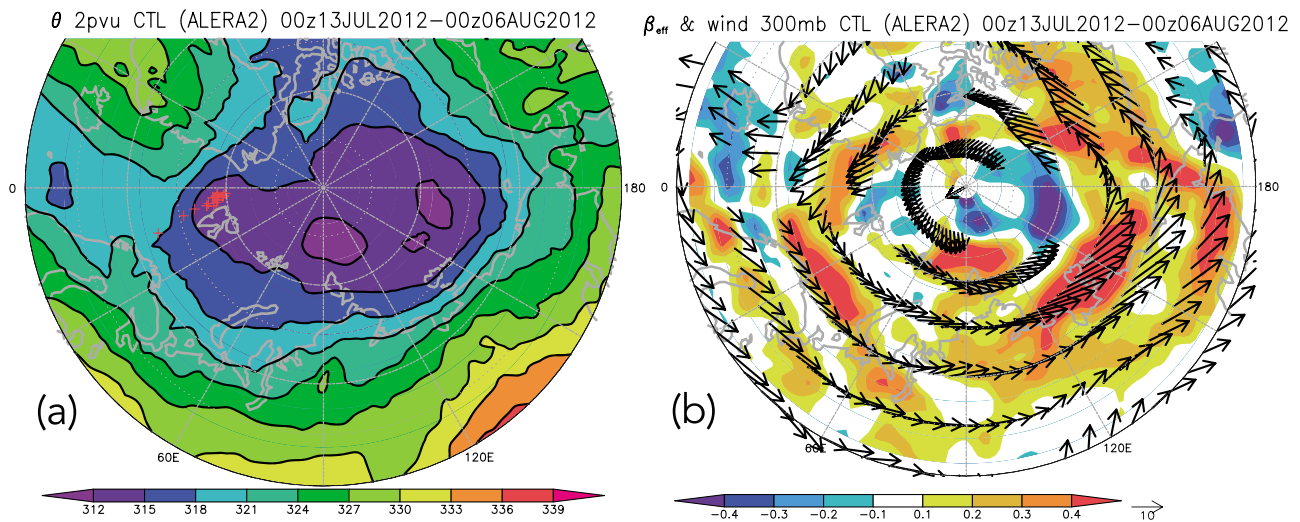


Figure 8. (a) Time-averaged θ_{dt} (K) and (b) effective β (PVU deg^{-1} ; meridional gradients of PV) and winds (m s^{-1}) at 300 hPa during 13 July to 6 August 2012, in CTL reanalysis. Red cross symbols in Figure 8a indicate locations of radiosonde observations during 13–29 July 2012.

amplitudes and they present similar tracks for AC12 and the TPV (not shown). However, in the different patterns of upper tropospheric circulation between the CTL and OSE, the TPV in the CTL is stronger than in the OSE at the developing stage (1–4 August) over mid-Eurasia, which is where and when AC12 starts to develop by baroclinic instability (Figure 10a). This pattern in turn implies that baroclinicity in the CTL is stronger than in the OSE for the development of AC12. Because the TPV in the CTL is stronger (with lower θ_{dt}) throughout the entire developing stage (2–5 August; Figure 10b), the stronger baroclinicity would be mainly caused by the difference in TPV strength.

The Eady growth rate, similar to *Simmonds and Rudeva* [2012], was calculated on jet core positions defined by wind speed maxima at 300 hPa over mid-Eurasia (Figure 10c). As expected, the Eady growth rate in the CTL is stronger than in the OSE on 2 August (0–24 h in relative time), just before the baroclinic growth of AC12 (Figure 9a). In summary, the CTL field has greater potential than the OSE for the baroclinic growth of AC12.

We verified which atmospheric fields of the CTL and OSE were more realistically simulated by comparing them with ERAI. Averaged vertical temperature errors of the CTL and OSE, relative to ERAI, were compared over the area of the *Polarstern* observations (shown in Figure 1), which is the region where the difference between the CTL and OSE was expected to originate (Figure 11).

The errors of both reanalyses look similar compared to ERAI, especially with regard to the positive temperature bias in the middle troposphere (Figures 11a and 11b). Although a similar bias has been found even in a regional forecasting model [*Cavallo and Hakim*, 2010], such a bias could also stem from model biases over the data-sparse regions [*Wesslén et al.*, 2014]. However, this bias does not stem from the *Polarstern* observations because it is common to both reanalyses. More importantly, a persistent negative temperature bias at the tropopause was found in the OSE from 20 to 27 July, which was not present in the CTL. Therefore, it can be concluded that the tropopause in the CTL is more realistically simulated than in the OSE during this period.

The average difference between the CTL and OSE over the same region (Figure 11c) shows large impacts in the upper troposphere, especially during mid-July. The large impacts near the tropopause are of the same characteristics as the OSE result of *Inoue et al.* [2013]. Furthermore, impacts of the observations persist even after July 29 when observations were suspended; July observations could influence on AC12 in early August.

Because a bias corresponds to an anomaly compared to the “real” field, i.e., ERAI in this case, it might transfer eastward via the upper tropospheric circulation by advection or propagation. In the OSE, the persistent bias at the tropopause could affect reproducibility downstream of the observation area, such as for the TPV over mid-Eurasia. Thus, in the OSE, the TPV might not be reproduced well; however, bias in the CTL has no effect because the CTL has a realistic tropopause during this period.

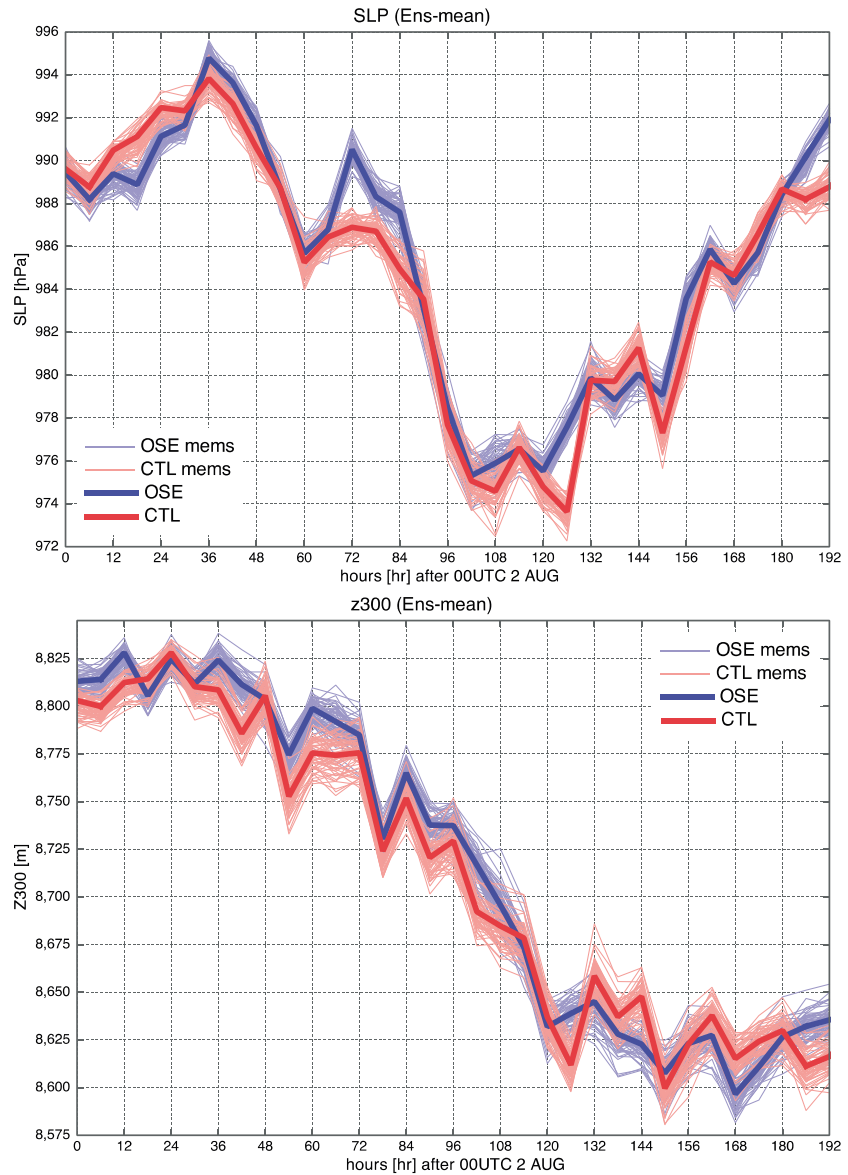


Figure 9. Time evolutions: (top) SLP (hPa) of the surface cyclone (AC12) center and (bottom) Z300 (m) of the TPV center in the CTL (red) and OSE (blue) analysis ensemble means. Light and thin lines show the time evolutions for 63 ensemble members. The centers of AC12 and the TPV are shown in Figure 2. The horizontal axis shows time (hours) relative to 00:00 UTC 2 August 2012.

We examine how the errors propagated downstream by observing the difference (response) between the CTL and OSE (CTL – OSE). The difference of the θ_{dt} field between the CTL and OSE is shown in Figure 12 for 21 July through 3 August, the period during which the persistent bias exists and just before AC12 starts to develop. A large-scale positive θ_{dt} response exists, corresponding to the positive geopotential height response in the upper troposphere over the Svalbard region (Figure 12b). There is a negative θ_{dt} response downstream because of propagation of the bias. The positive θ_{dt} response stems from the negative persistent bias of the OSE in Figure 11b, because the CTL is more realistic over this region. The negative θ_{dt} response is just over central Eurasia. This response corresponds to the negative Z300 anomaly (pattern) of the TPV during the developing stage of AC12 (Figure 10a), because a negative θ_{dt} anomaly conversely corresponds to a negative geopotential height anomaly as in Figure 12b. Thus, it can be concluded that in the CTL, the TPV is stronger and more realistic during the developing stage of AC12 than in the OSE. This difference originates from the temperature bias at the tropopause in the OSE over the Svalbard region, where

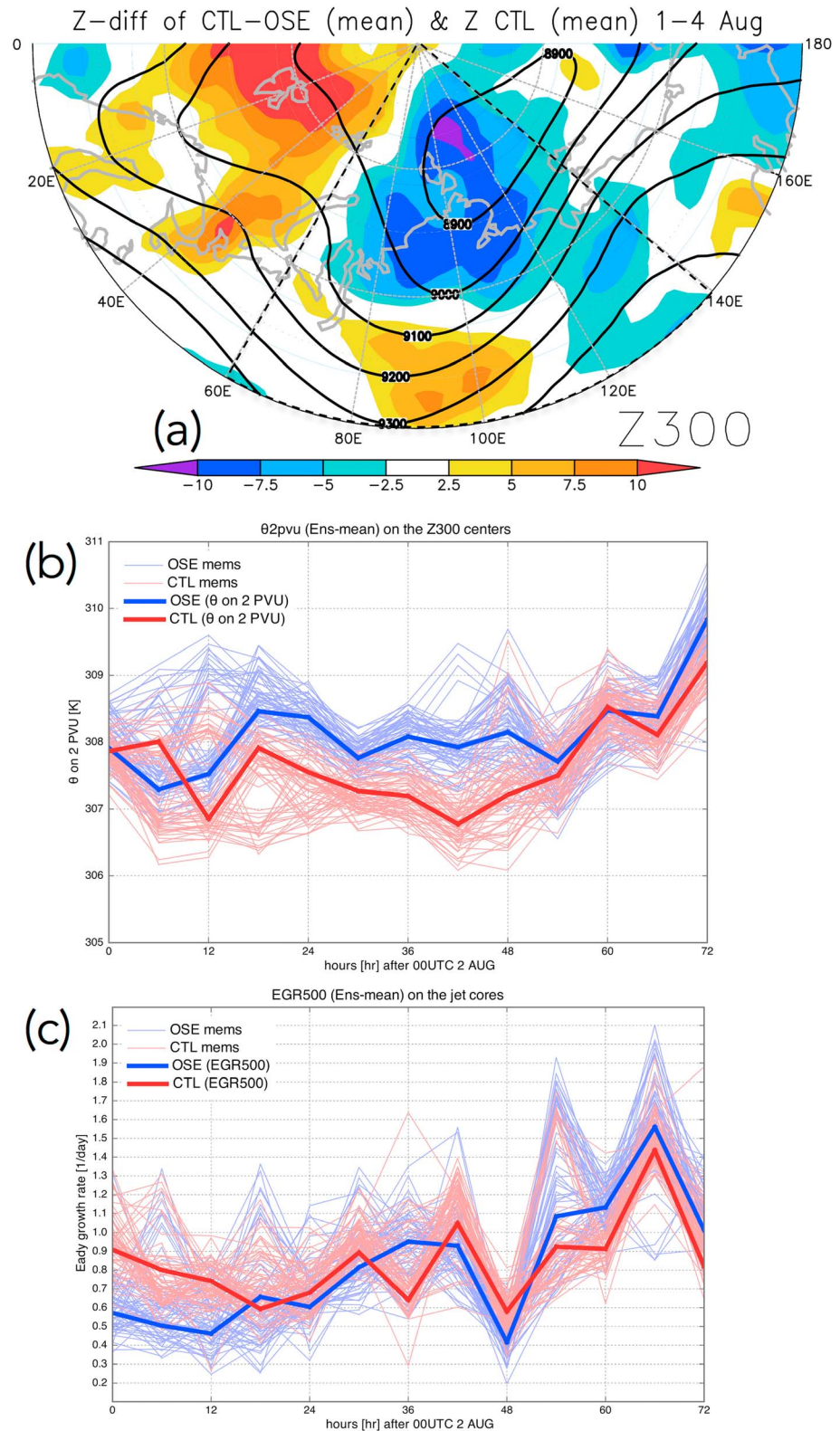


Figure 10. (a) Average differences (shading) and fields in the CTL (contours) in Z300 (m) between CTL and OSE during developing stage (1–4 August). A spherical triangle (square in a cylindrical map projection) shown by dashed black line indicates region for piecewise PV inversion. Same as Figure 9 but for (b) the area-average θ_{at} within radius of 500 km centered on the TPV centers and (c) Eady growth rates (day^{-1}) at the jet core centers in the CTL (red) and the OSE (blue). See text for more details.

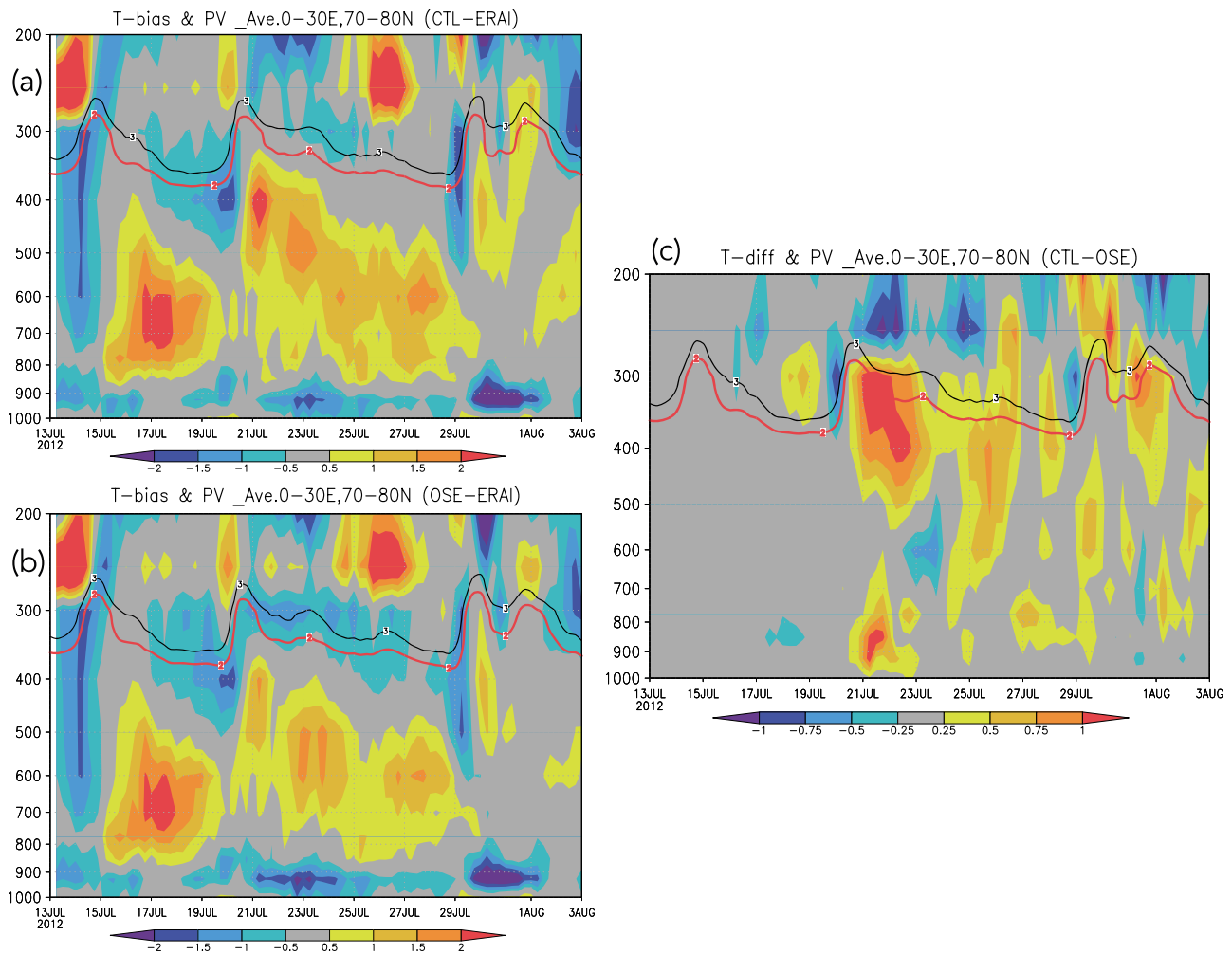


Figure 11. Area-averaged vertical distributions of temperature differences (errors; shading; °C) between the (a) CTL and (b) OSE against ERAI (CTL or OSE – ERAI) and PV (PVU), averaged over the *Polarstern* observation area during 00:00 UTC 13 July to 00:00 UTC 3 August 2012. The area is indicated by the yellow outline in Figure 1. The tropopause is indicated by the red lines (2 PVU surface), and the black lines indicate the 3 PVU surface. (c) Same as Figure 11a but for temperature difference between CTL and OSE (CTL – OSE).

the *Polarstern* observations have direct impact on improved simulation of the atmospheric circulation. Furthermore, these results indicate that errors in the reproducibility of the tropopause would propagate rather than be advected via the PV gradient on the tropopause (Figure 8b).

To further demonstrate the error propagation, time sequences of the negative θ_{dt} response at Svalbard and positive θ_{dt} response in central Eurasia region are shown. Since air parcels move along an iso-PV surface under adiabatic conditions such as the upper troposphere, we only focus on area averages on the dynamical tropopause there (Figures 13a and 13b). The average regions for the positive and negative θ_{dt} responses are defined as the zones bounded by 70°N–90°N and 0°E–40°E, and 70°N–90°N and 80°E–120°E, respectively. The former is called the upstream region and the latter the downstream region. Additionally, a time sequence of average zonal wind across the region intermediate to those two regions (70°N–90°N, 20°E–100°E) is shown (Figure 13c) to estimate the error propagation speed.

The responses/errors (CTL – OSE) over the upstream and downstream regions are quantified by the difference in kinetic energy DKE between CTL and OSE as

$$DKE \equiv \frac{1}{2} [(u_{CTL} - u_{OSE})^2 + (v_{CTL} - v_{OSE})^2], \quad (1)$$

where u and v are the zonal and meridional winds, respectively, and subscripts CTL and OSE indicate the reanalyses. Temporal DKE evolution in the two regions indicates that the response (DKE) in the upstream

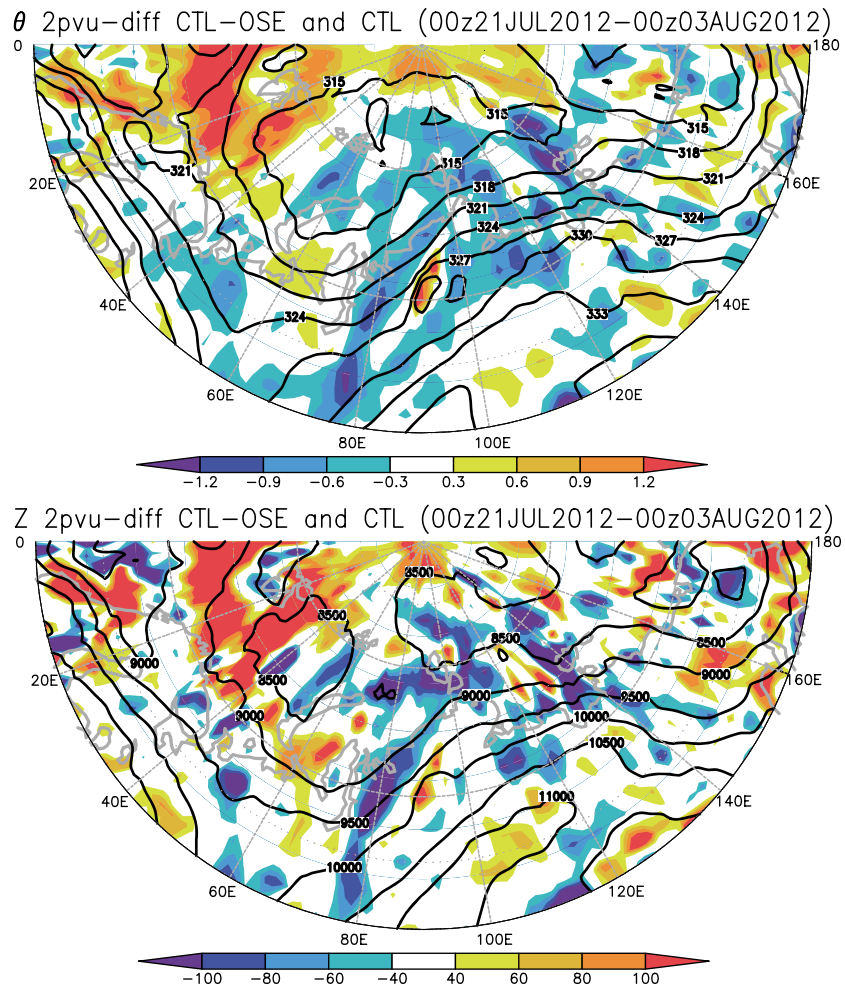


Figure 12. Same as Figure 10a but for (top) θ_{dt} (K) and (bottom) geopotential height (m) anomalies (CTL – OSE) on the 2 PVU surface, averaged from 00:00 UTC 21 July to 00:00 UTC 3 August 2012.

region precedes by about 1–3 days than that in the downstream region (Figure 13a), suggesting that the response to the *Polarstern* observations over the Svalbard region modified the response over central Eurasia. The lag between the two responses is consistent with the propagating time scale of wind speeds ~ 6 to 12 m s^{-1} (Figure 13c) or a group velocity speed generally faster than the wind speeds [e.g., Hoskins and James, 2014] at 80°N (i.e., ~ 3 to 1.5 days). The responses persist after 29 July as in Figure 11c.

Figure 13b shows area-average θ_{dt} in both regions. We see that the responses in these regions are anticorrelated and thus show opposite temperature responses at the tropopause. This result supports that the responses/errors propagated rather than advected. In addition, the responses keep the same polarities after 21 July, indicating that the errors propagated as a forced, stationary Rossby wave from a wave source of the *Polarstern* observation points. We can also see in Figure 13c that wind speeds in the CTL and OSE are almost the same, implying that a response would act as a perturbation in the tropopause, which is compatible with the linear theory of Rossby wave propagation. In summary, we conclude that errors without the observations over the Svalbard region could propagate as a stationary Rossby wave downstream of the central Eurasia region.

5. Forecast Experiments

Apart from data analyses described above, we conducted forecast experiments. Because the CTL and OSE are reanalysis data sets, they can be used as initial values for these forecast experiments. A 5 day integration was performed in the experiments.

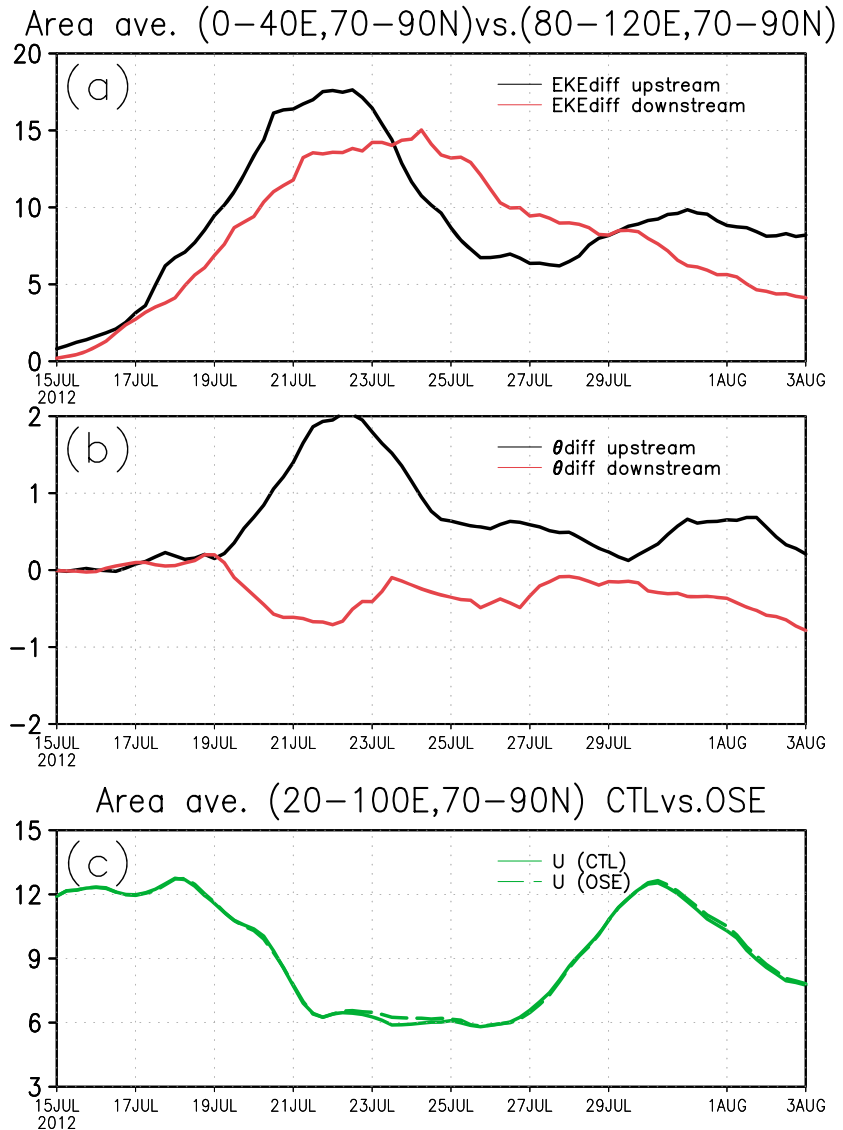


Figure 13. Temporal evolution of area-averaged differences between CTL and OSE (CTL – OSE) in (a) kinetic energy of the differential wind speeds $\frac{1}{2} [(u_{CTL} - u_{OSE})^2 + (v_{CTL} - v_{OSE})^2]$ ($m^2 s^{-2}$) at 2 PVU; (b) θ_{dt} (K) over the upstream region of 70°N–90°N and 0°E–40°E (black) and the downstream region of 70°N–90°N and 80°E–120°E (red); and (c) area-averaged zonal winds u_{CTL} and u_{OSE} at 2 PVU in CTL (solid green curve) and OSE (dashed green) across the intermediate region of 70°N–90°N and 20°E–100°E between the upstream and downstream regions. All temporal evolutions were filtered with 3 day running average to reduce noise.

Since both the CTL and OSE are the ensemble reanalyses with 63 members, we made ensemble forecasts with the same members, called CTL_{EPS} (Ensemble Prediction System from the CTL reanalysis) and OSE_{EPS} (Ensemble Prediction System from the OSE reanalysis). In addition, other initial values were used for the forecast experiments, that is, ERAI and modified CTL for which some parts of PV distributions in the upper and lower troposphere replaced those in the OSE.

All experiments used the same forecast model (AFES) with the same configuration for ALEDAS2. Thus, only initial values were different in all the experiments. The experiment with the ERAI initial condition had a single forecast and not an ensemble, so we call this experiment the Deterministic Prediction System (DPS) instead of EPS. Details of the experiments are summarized in Table 1.

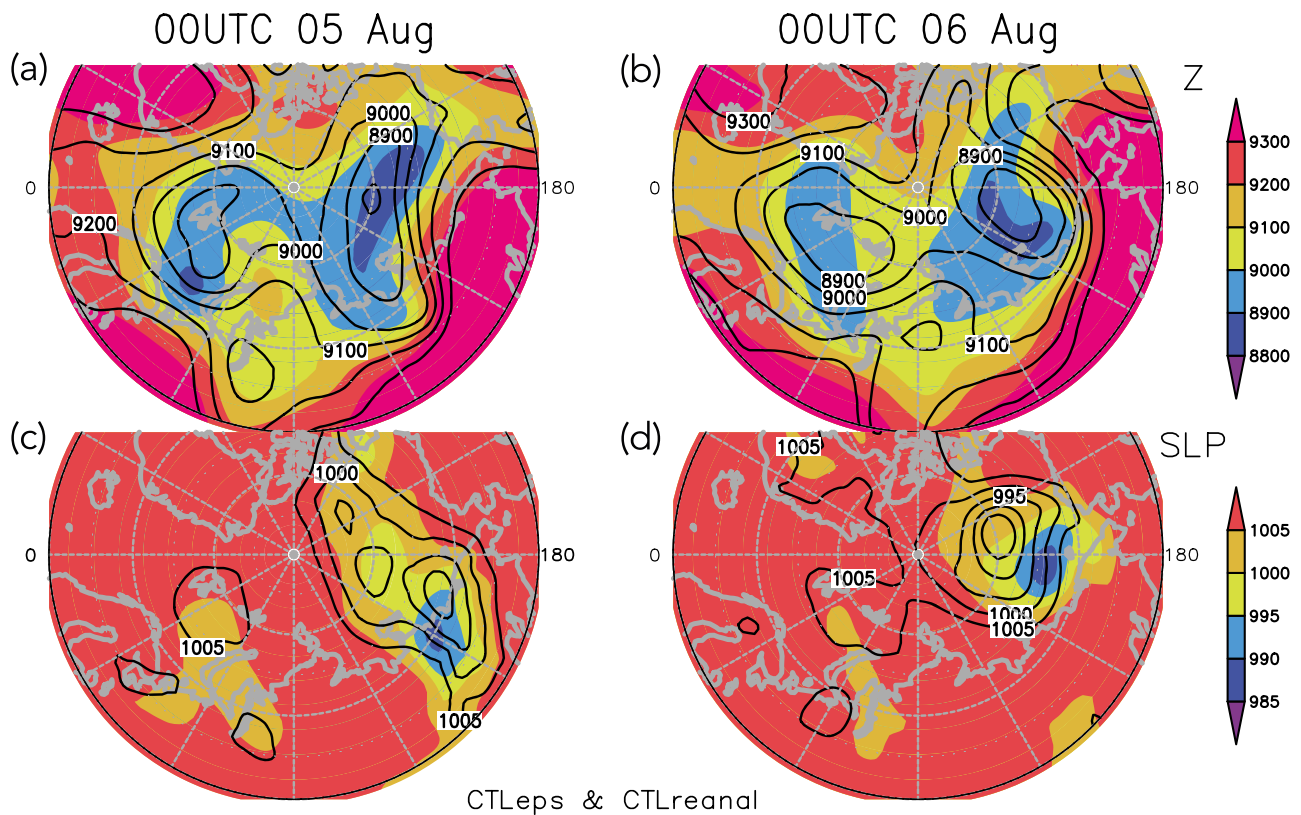


Figure 14. Z300 (m) and SLP (hPa) at (a and c) 00:00 UTC 5 August and (b and d) 6 August 2012 of the CTL analysis ensemble mean (contours) and CTLEPS ensemble mean (shading) fields. The dates for the CTLEPS indicate valid dates, i.e., the dates 5 and 6 August correspond to the 2 and 3 day forecasts, respectively.

5.1. Forecasts From CTL and OSE Reanalyses

Ensemble forecasting experiments, using the CTL and OSE as the initial values, were conducted to clarify the impact of the small amplitude difference between the CTL and OSE reanalysis fields on the prediction of AC12. The atmospheric fields of the CTL and OSE at 00:00 UTC on 3 August 2012 were used as the initial values for the forecasting experiments, because soon thereafter, AC12 began to develop by baroclinic instability. The experiments using the CTL and OSE as the initial values are hereafter called the CTLEPS and the OSEEPS, respectively.

Figure 14 shows that in comparison with the CTL, the CTLEPS fields of Z300 and SLP can reproduce the developments of the TPV and AC12 for 2 and 3 day forecasts. In the Z300 field, the CTLEPS captures the southward intrusion of the TPV over mid-Eurasia near the Laptev Sea, and thus the ensuing baroclinic instability. In the SLP field, amplification of AC12 can be found in the CTLEPS, similar to the CTL. Although their central positions appear different, AC12 trajectories in the CTLEPS and CTL are similar. Hence, the CTLEPS reproduces well the formation of AC12 and its surrounding circulations in the upper and lower troposphere reasonably well.

Figure 15 shows that the OSEEPS field cannot capture well the formation of AC12. In this figure, the difference in reproduction (reproducibility) between the CTLEPS and OSEEPS is identified as the difference of the CTLEPS against the OSEEPS ($CTL_{EPS} - OSE_{EPS}$). In the SLP field (Figures 15c and 15d), the amplitude of AC12 is smaller by ~ 7.5 hPa in the OSEEPS than in the CTLEPS. Moreover, because the central positions of AC12 in the CTLEPS and OSEEPS are almost the same, the difference in the SLP reproduction does not indicate a difference in AC12 position between the CTLEPS and OSEEPS. In the Z300 field (Figures 15a and 15b), a negative reproducibility appears at the TPV, which implies that the baroclinic instability necessary for the formation of AC12 is significantly weaker in the OSEEPS.

We examined time sequences of AC12 vertical distribution in the CTLEPS and OSEEPS (Figure 16). By comparing the reanalysis CTL, both the CTLEPS and OSEEPS reproduce the baroclinic structure in the

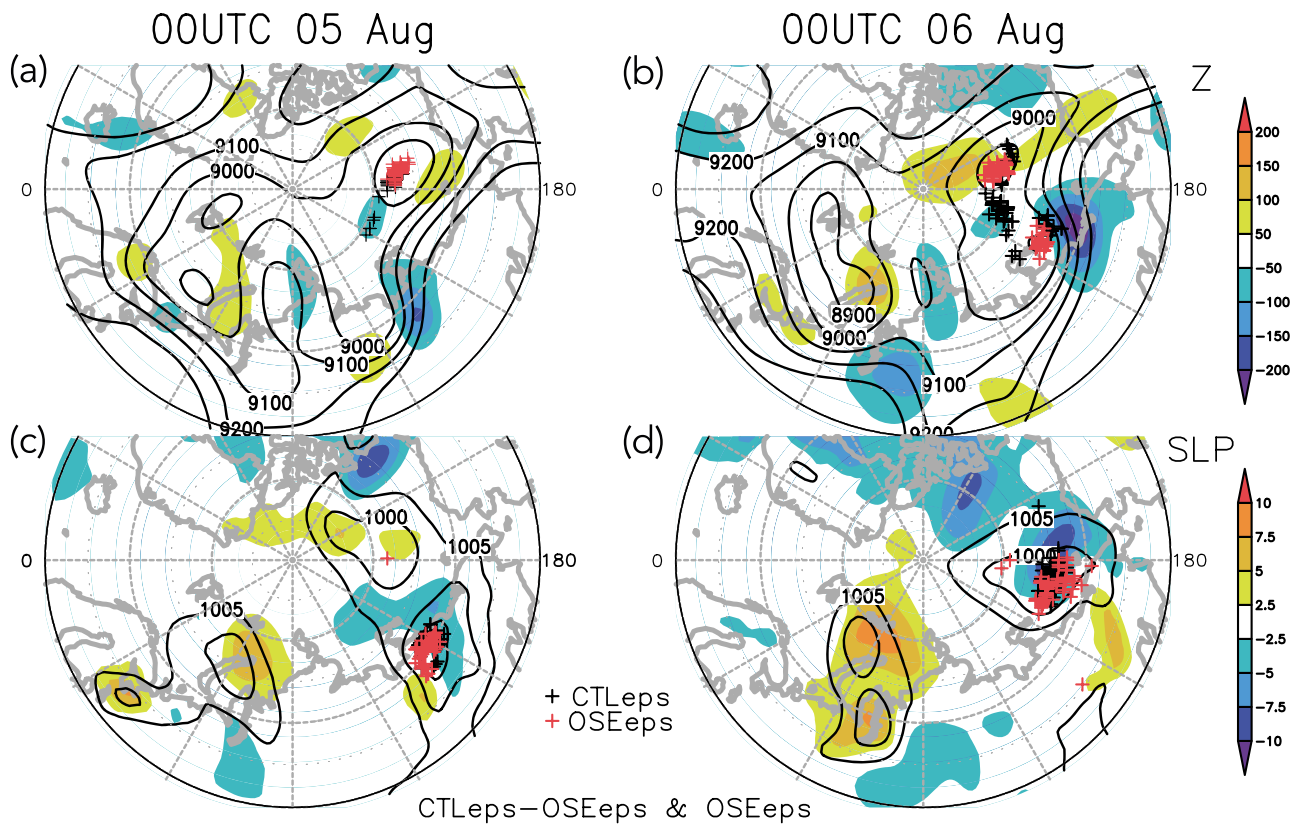


Figure 15. Same as Figure 14 but for the differences in Z300 (m) and SLP (hPa) between the CTL_{EPS} and the OSE_{EPS} (CTL_{EPS} – OSE_{EPS}; shading). The contours indicate the OSE_{EPS} fields. Black and red cross symbols are the TPV and the AC12 centers in the CTL_{EPS} and the OSE_{EPS}, respectively.

developing stage as well as the warm core in the upper troposphere and cold core in the lower [Tanaka *et al.*, 2012] in the mature stage. Also, cyclone tracks in both experiments are well reproduced. There is a marked difference between the CTL_{EPS} and OSE_{EPS} in the strength of the warm core around 6 August, when AC12 just became equivalent barotropic. The warm core corresponds to the TPV and the marked difference is in its strength. Because the TPV originally developed with AC12 by baroclinic instability during the developing stage (Figure 15), we conclude that AC12 formation in the OSE_{EPS} from this instability is substantially weaker than that in the CTL_{EPS}. Note that although another process might exist to develop the TPV together with baroclinic instability, as suggested by Tanaka *et al.* [2012] who highlighted the merging of smaller-scale mesocyclones, such a process could support baroclinic instability because the process could act to enforce the surface cyclone (AC12) and/or the TPV.

Temporal evolution of AC12 amplitudes in the CTL_{EPS} and OSE_{EPS} is depicted in Figure 17. The time evolution in the CTL_{EPS} reproduces the amplification and time sequence of AC12 in the CTL reanalysis, whereas the time evolution in the OSE_{EPS} does not reproduce the amplification. As discussed above, because almost all ensemble members of the centers of AC12 (surface cyclone) in the CTL_{EPS} and OSE_{EPS} are located close to each other throughout the entire 5 day integration (not shown), the AC12s in these EPSs have different amplitudes rather than different positions. Because the amplitude in the OSE_{EPS} is smaller than in CTL_{EPS} and temporal evolution in the former is significantly different than that in the latter, we conclude that the OSE_{EPS} cannot simulate well the AC12 formation.

Although the CTL_{EPS} successfully reproduces the formation of AC12, its rapid intensification (e.g., minimum value of central SLP) is too weak compared with the CTL, in which SLP reached ~974 hPa and maintained this value during 6 and 7 August. One reason may be that the surface cyclone with the weaker amplitude over the Arctic Ocean merges with AC12 in the CTL_{EPS} (Figure 14c). Because AC12 has a barotropic structure during the mature stage (after 6 August), its intensification by the horizontal vortex merger [Aizawa *et al.*, 2014] may be weaker in the CTL_{EPS}.

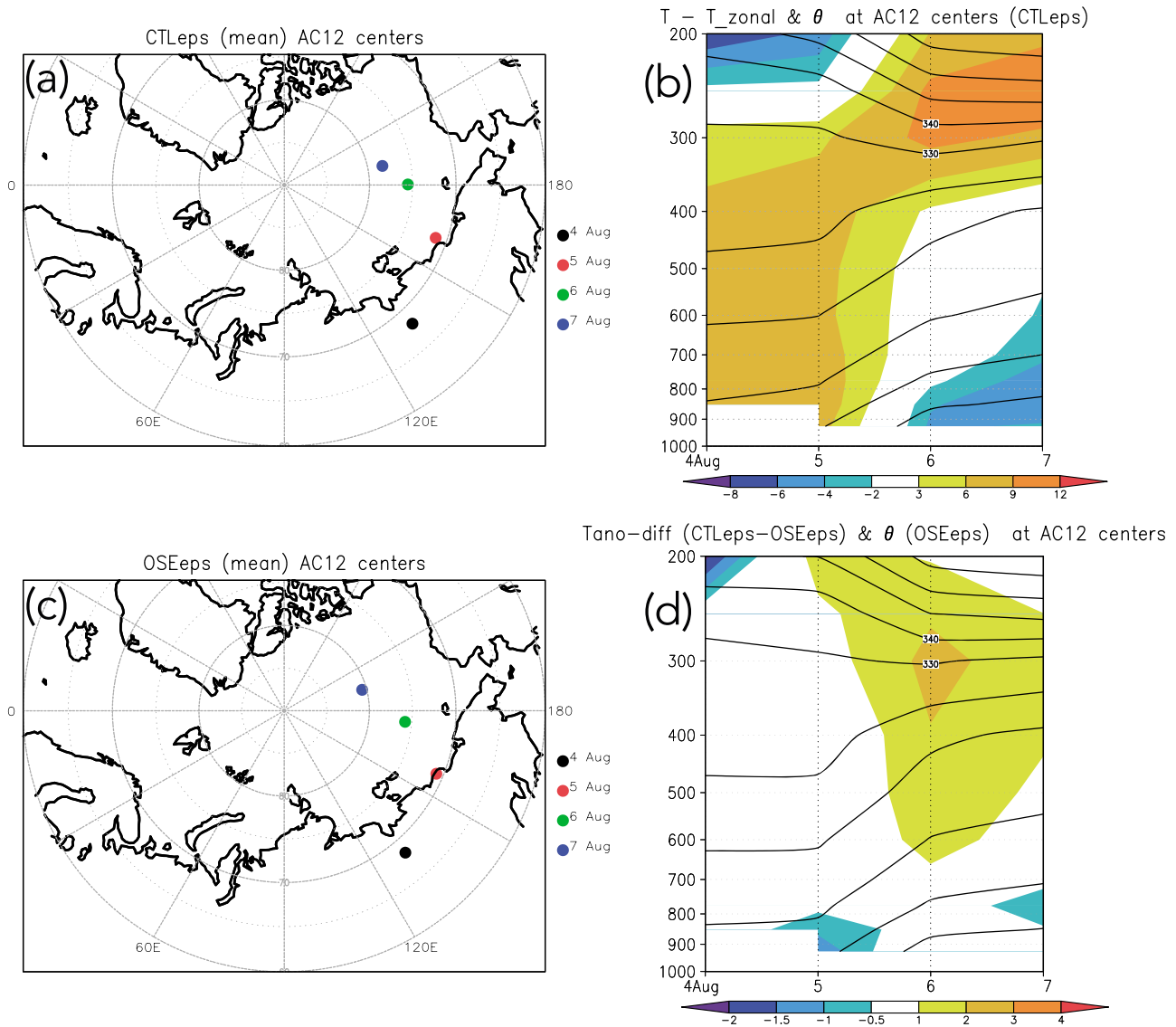


Figure 16. Same as Figure 4 but for the ensemble mean fields of (a and b) CTL_{EPS} and (c and d) OSE_{EPS}, except that shading in Figure 16d indicates difference between CTL_{EPS} and OSE_{EPS} (CTL_{EPS} – OSE_{EPS}).

We further conducted a deterministic (single) forecasting experiment using AFES with the same configuration as the CTL_{EPS}, except for using ERAI as the initial values (Table 1). This experiment is denoted ERAI_{DPS}. It is found that the time evolution in the ERAI_{DPS} reproduces the amplification as well the CTL_{EPS} does, which implies that a realistic representation of the large-scale upper tropospheric circulation in the Arctic region is crucially important for the prediction of disturbances such as strong Arctic cyclones.

The small amplitude, but large-scale reproducibility between the CTL and OSE in the initial fields during the initial developing stage cause large prediction errors for AC12. The results show that the radiosonde observations by *Polarstern*, which causes realistic reproduction of the large-scale upper tropospheric circulation in the Arctic region, had significant impact on the prediction of AC12.

5.2. Relative Importance of the Reproducibility of the TPV and Surface Baroclinicity

One question to be answered is whether reproducibility in the upper troposphere (TPV) is more important than that in the lower troposphere (surface baroclinicity) for the prediction of AC12. This was examined by isolating the reproducibility stemming from the TPV and surface baroclinicity between the CTL and OSE. As

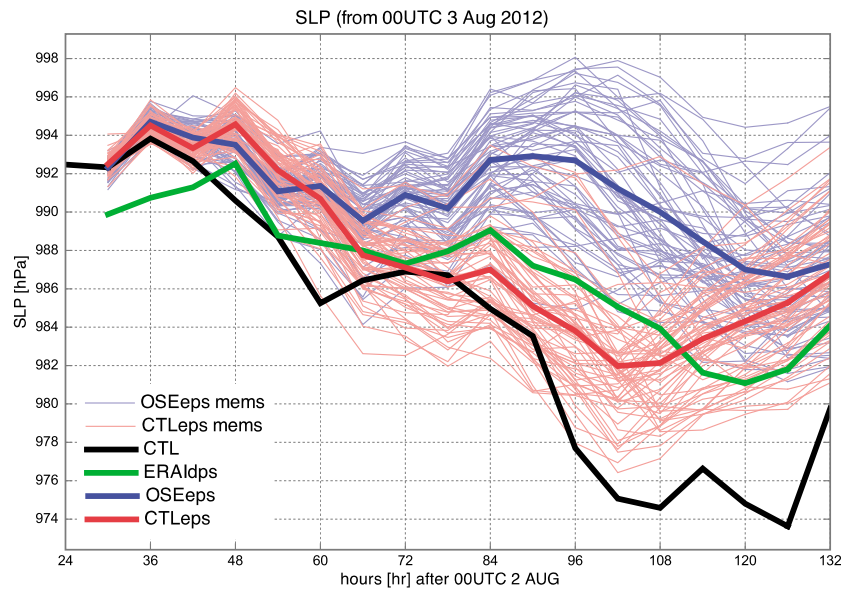


Figure 17. Same as Figure 9a but for the CTL Ensemble Prediction System (CTL_{EPS}) experiment (red) and the OSE_{EPS} (blue). Light and thin lines indicate temporal evolutions of all 63 ensemble members of CTP_{EPS} (red) and OSE_{EPS} (blue). The thick red and blue lines indicate the ensemble means of minimum SLP at AC12 centers of the ensemble members. Time evolutions in the CTL reanalysis (black) and ERAI Deterministic Prediction System experiment (ERA_{DPS}, green) are also shown.

the focus of this work is on the reproducibility at the upper troposphere, in association with the additional radiosonde observations, answering the above question makes our conclusions more robust.

Forecasting experiments similar to the CTL_{EPS} were performed, except the reproducibilities in the initial values between the CTL and OSE (CTL – OSE) were subtracted individually in the upper or lower troposphere over mid-Eurasia where AC12 started to develop. That is, the TPV or surface baroclinicity in the CTL (initial value) was replaced by that in the OSE. Through the experiments, the relative contributions of the TPV and surface baroclinicity reproducibilities to the prediction of the development of AC12 in the CTL_{EPS} were estimated. Before the forecasting experiments were performed, the reproducibilities between the CTL and OSE at the initial values were determined, in terms of PV and θ , which are useful for decomposing the atmosphere into areal “partitions” [Bishop and Thorpe, 1994]. Figure 18 shows the meridional-vertical cross sections of the differences in the triangle region (mid-Eurasia) displayed in Figure 10a, which is when and where AC12 started to develop. It can be seen that both the PV and θ fields have relatively large reproducibilities around and over the tropopause and near the North Pole. AC12 developed at around 75°N (i.e., the Russian coast) and the differences in the upper troposphere relative to the lower troposphere at this latitude are large.

To conduct the forecasting experiments, the initial values of wind, geopotential height, and temperature fields stemming from the reproducibilities of the TPV and surface baroclinicity (anomalies) were required. To obtain the fields, a piecewise PV inversion was conducted [Davis and Emanuel, 1991]. The method is based on two ideas concerning PV. The first considers that PV or the surface θ can be decomposed into some partitions related to region or amplitude and thus can be superimposed [Bishop and Thorpe, 1994]. The other considers that PV and the surface θ can be converted into wind, temperature, and geopotential fields balanced with them (the PV “invertibility principle” [Hoskins et al., 1985]), which is the PV inversion process. Following the two ideas, the reproducibility is divided into two partitions of the upper and lower troposphere over mid-Eurasia. The former is related to the difference of the TPV between the CTL and OSE, while the latter is that of the surface baroclinicity. By treating the reproducibilities of the pieces as a PV or surface θ anomaly, differences in the wind, temperature, and geopotential anomaly fields with respect to their initial values can be obtained, which correspond to the reproducibility of the TPV (upper troposphere) or surface baroclinicity (lower troposphere). The two pieces were divided as follows. We used the difference in the PV and surface θ between the CTL and OSE at 00:00 UTC on 3 August. The upper piece was the difference of PV between heights of 500 and 100 hPa over mid-Eurasia (the triangle region in Figure 10a), and the lower piece was the difference of PV between heights of 925 and 600 hPa and θ at 1000 hPa (the surface). For

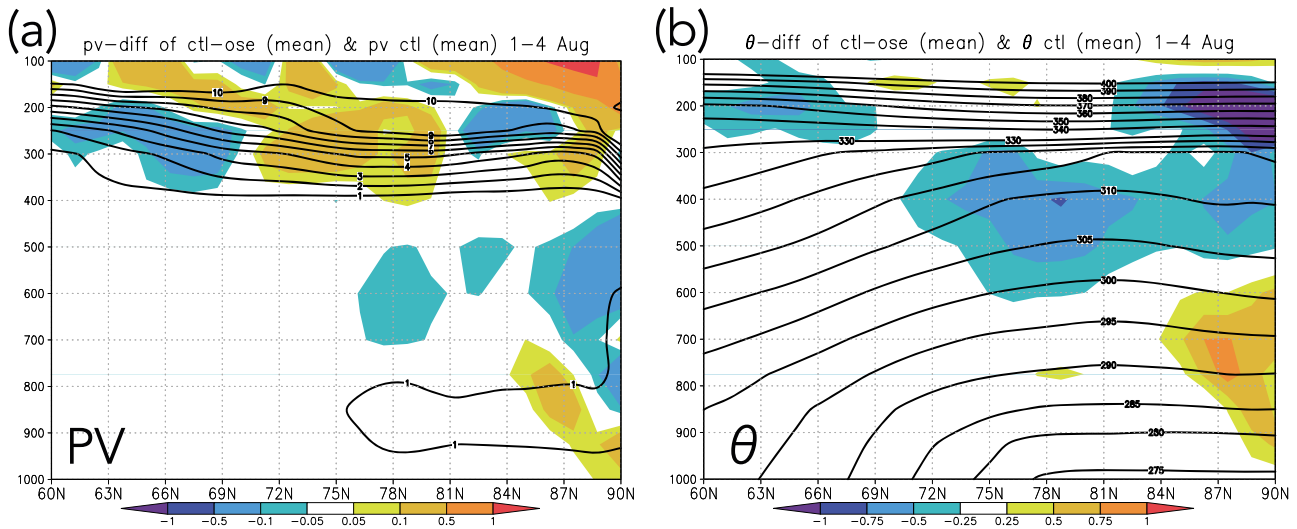


Figure 18. Same as Figure 10a but for pressure-latitude cross sections of the reproducibilities (CTL – OSE) of the zonally averaged (a) PV (PVU) and (b) θ (K) over the triangle region shown in Figure 10a. Contours are for 1–10 PVU and 275–400 K.

each piece, the PV value out of its heights and region was set to 0. For the PV inversion process to obtain the balanced fields, we used a quasi-geostrophic (QG) PV framework. Details of this approach are provided in the Appendix A.

Figure 19 shows the balanced fields with the upper and lower PV and surface θ anomalies. It can be seen that the upper anomaly contributes to the westerly flow in the upper troposphere over central Eurasia and thus intensifies the baroclinicity, whereas the lower anomaly contributes little to the change in baroclinicity in either the upper or the lower troposphere.

Balanced fields for each anomaly (reproducibility of the TPV or the surface baroclinicity) were subtracted from the initial values of the CTL_{EPS} at 00:00 UTC on 3 August. These subtracted values were used as the initial values for the forecasting experiments of the CTL_{EPS}, in which the upper and lower level circulations

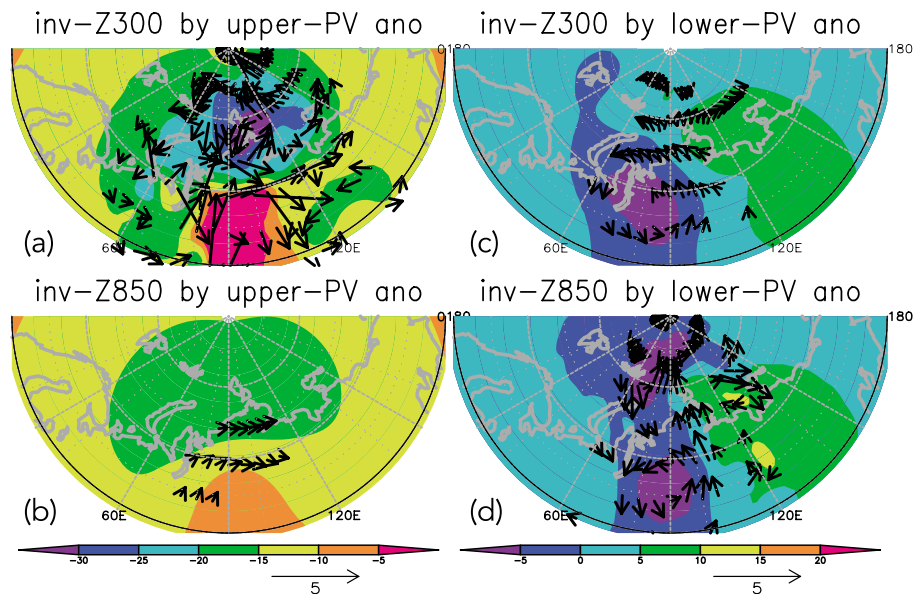


Figure 19. Geopotential height (shading; m) and wind (vectors; m s^{-1}) anomaly fields “induced” by (balanced with) the (a and b) upper PV (the upper anomaly; see text for more details) and (c and d) lower PV and surface θ (the lower anomaly) anomalies at 00:00 UTC 3 August 2012. The fields are at 300 and 850 hPa.

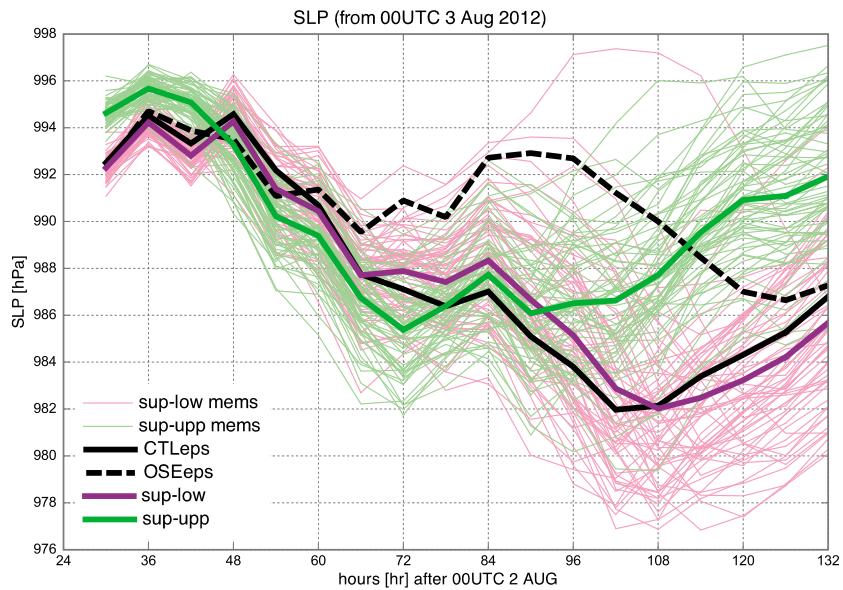


Figure 20. Same as Figure 17 but for the experiment suppressing the upper anomaly (sup-up Exp, green lines) and the sup-low Exp (purple lines). See text for more details. Light and thin lines indicate temporal evolutions of ensemble members. Black lines indicate the time evolutions of the CTL_{EPS} (solid) and OSE_{EPS} (dashed) ensemble means.

over mid-Eurasia were replaced by the OSE. Hereafter, the former experiment is denoted as the sup-up Exp (experiment suppressing the upper anomaly) and the latter as the sup-low Exp (experiment suppressing the lower anomaly). Our goal is to determine which experiment the development of AC12 is suppressed.

The time evolution of the amplitude of AC12 in the sup-up Exp is significantly different from the CTL_{EPS}, while that in the sup-low Exp is not (Figure 20). Although AC12 developed in both Exps during the early developing stage (until 72 h), the amplitude in the sup-up Exp subsequently becomes weaker compared with the CTL_{EPS}. However, the time evolution in the sup-low Exp is similar to that in the CTL_{EPS}. Therefore, the reproducibility of the TPV is more important than that of surface baroclinicity for predicting the development of AC12. This result again supports the assertion that additional radiosonde observations can affect the prediction of the surface AC12 via the upper tropospheric circulation.

6. Conclusions

The impact of radiosonde observations in the Arctic region on the prediction of the “great” August 2012 Arctic cyclone (AC12) is assessed using an observing system experiment (OSE). The observations were performed by the German research vessel *Polarstern* cruising near the Svalbard during mid-July to early August 2012. For the experiment, an atmospheric ensemble reanalysis (ALERA2) was used as the control experiment (CTL), which could satisfactorily reproduce AC12 and the large-scale surrounding fields. The OSE used the same reanalysis data as the CTL, except that the OSE did not include the radiosonde observations from the *Polarstern*.

The formation of AC12 reflected typical baroclinic growth in mid-Eurasia, where baroclinicity is large because of the thermal contrast between the warm Eurasian continent and cold Arctic Ocean. When the AC12 started to develop, a TPV supported the baroclinic growth. The TPV was advected from a northern region with high-PV and triggered baroclinic instability when it arrived over the baroclinic zone of mid-Eurasia. AC12 developed by moving northeastward along the zone and it matured after encountering the Arctic Ocean.

The CTL and OSE reanalyses were compared to evaluate the impact of the radiosonde observations on AC12. A small amplitude difference in the reproduction (reproducibility) of the TPV was found between them. The TPV was not reproduced as well in the OSE, with a weaker amplitude of the TPV when AC12 started to develop. The CTL fields showed conditions more favorable for baroclinic instability. In addition, the CTL was

more realistic at the tropopause than the OSE was. The reproducibility between the CTL and OSE (CTL – OSE) at the tropopause propagated from the upstream region where the observations were performed by the research vessel *Polarstern*.

The impact on forecasts of AC12 was examined using ensemble forecast experiments. These experiments were conducted using the CTL and OSE as initial values just before AC12 started to develop. The forecast from the CTL reproduced the formation of AC12 by baroclinic instability, while that from the OSE produced a significantly weaker cyclone. To establish that the reproducibility of the TPV was more important for the prediction of AC12 than the surface baroclinicity in the lower troposphere, the relative contributions to the AC12 development of the reproducibilities of the upper and lower troposphere (between the CTL and OSE) were quantified using sensitivity forecast experiments. In the sensitivity experiments, the initial values in the upper or lower troposphere were replaced by the OSE values using the piecewise PV inversion method. The results showed that the reproducibility of the TPV was more important for the prediction of the development of AC12.

In summary, the radiosonde observations performed by the *Polarstern* were essential for the prediction of AC12. Even though the observations were taken far from the location of AC12, they remotely affect the predictions of AC12 via the reproducibility of the large-scale upper tropospheric circulation in the Arctic region. One suggestion from the present study is that upper air measurements by radiosondes are important for reproducing Arctic atmospheric circulations, by adding significant vertical information compared to Arctic drifting buoys on the surface [Inoue *et al.*, 2009]. As sea ice cover prevents cruises on the Arctic Ocean during winter, more intense vertical profile and upper air observations in the Arctic coastal regions seem eligible.

Through this study, it is established that even a few radiosonde observations from one research vessel can have considerable influence on the forecasting of an Arctic cyclone, which was one of the most intense disturbances in the polar region since records began. Even now, few upper air observations are performed over the Arctic region due to the limited number of observing stations or cruises of research vessels that can launch radiosondes [Lüpkes *et al.*, 2010]. An increase in the number of such observations could improve the prediction and reproduction of individual disturbances and climatic fields within the Arctic region, as well as those in lower latitudes [Inoue *et al.*, 2013; Jung *et al.*, 2014]. Such an improvement would be very helpful for future polar and global climate research, as mentioned in the introduction. Another possibility is for predicting the feasibility and effectiveness of the Northern Sea Route [Khon *et al.*, 2014] on weather and synoptic time scales. Successful forecasting of an Arctic cyclone would especially aid cruises along the route.

Appendix A: Piecewise Quasi-Geostrophic PV Inversion Method

The balanced fields with the PV and the surface θ anomaly fields were obtained using the PV inversion method within the quasi-geostrophic (QG) framework [Takaya and Nakamura, 2005]:

$$\psi \equiv L_g^{-1} q = \left[\nabla^2 + \frac{f_0^2}{\rho_0} \frac{\partial}{\partial z} \left(\frac{\rho_0}{N^2} \frac{\partial}{\partial z} \right) \right]^{-1} q, \quad (\text{A1})$$

where ψ and q are the stream function and QG PV anomalies, respectively, and L_g^{-1} indicates the inverse Laplacian-like operator, ∇^2 is the Laplacian operator in spherical coordinates, f_0^2 is the Coriolis parameter at 75°N, $\rho_0 = \rho_s \exp(-z/H_s)$ ($\rho_s = 1.452 \text{ kg m}^{-3}$), $z = -H_s \ln(p_0/p)$ (where $H_s = 7025 \text{ m}$, $p_0 = 1000 \text{ hPa}$, and p is pressure at each level), and $N^2 = R/H_s (d\bar{\theta}/dz) \exp(-\kappa z/H_s)$ ($R = 287 \text{ J K}^{-1} \text{ kg}^{-1}$, $\kappa = 0.286$, and $\bar{\theta}$ represents potential temperature at each level averaged over the northern side of 60°N). Here $\psi = \phi/f_0$, where ϕ is the geopotential anomaly. For the inversion procedure, the spherical harmonic expansion was adopted, as in Takaya and Nakamura [2005]. The triangular truncation used here is 95 (approximately 1.25° intervals). Calculation of the inversion was performed over the entire globe and within the heights between 1000 and 10 hPa. The lateral boundary condition was set to be periodic prescribed by the spherical harmonic expansion, and the upper boundary (at 10 hPa) was set to be zero θ anomaly (homogeneous Neumann condition), i.e., $\partial\psi/\partial z = 0$, respectively. The lower boundary (at 1000 hPa) condition was the homogeneous Neumann condition for the upper piece, and the inhomogeneous condition, in which the reproducibility of the surface θ between the CTL and OSE, was given for the lower piece. Note that the lower boundary condition employed here was that commonly used for the piecewise PV inversion method [e.g., Davis and Emanuel, 1991].

Acknowledgments

The ALERA2 data set can be available from <http://www.jamstec.go.jp/esc/research/oreda/products/index.html>. PREPBUFR compiled by the National Centers for Environmental Prediction (NCEP) and archived at the University Corporation for Atmospheric Research (UCAR) is used as the observations (available from <http://rda.ucar.edu>). The detailed information for the *Polarstern* radiosonde data, see König-Langlo [2012]. This work was supported by funds from Grant-in-Aid for Scientific Research (24241009 and 25800267). The authors thank Nobumasa Komori, Takeshi Enomoto, Akira Kuwano-Yoshida, Wataru Yanase, Eigo Tochimoto, Keita Iga, and Takemasa Miyoshi for stimulating discussions and three anonymous reviewers for their comments. ALEDAS2 and AFES integrations were performed on the Earth Simulator with the support of JAMSTEC. Figures were drawn using GrADS and MjoGraph.

References

- Aizawa, T., H. L. Tanaka, and M. Satoh (2014), Rapid development of arctic cyclone in June 2008 simulated by the cloud resolving global model NICAM, *Meteorol. Atmos. Phys.*, *126*, 105–117, doi:10.1007/s00703-013-0272-6.
- Ambaum, M. P. H., B. J. Hoskins, and D. B. Stephenson (2001), Arctic Oscillation or North Atlantic Oscillation?, *J. Clim.*, *14*, 3495–3507, doi:10.1175/1520-0442(2001)014<3495:AONAO>2.0.CO;2.
- Barnston, A. G., and R. E. Livezey (1987), Classification, seasonality and persistence of low-frequency atmospheric circulation patterns, *Mon. Weather Rev.*, *115*, 1083–1126, doi:10.1175/1520-0493(1987)115<1083:CSAPOL>2.0.CO;2.
- Bishop, C. H., and A. J. Thorpe (1994), Potential vorticity and the electrostatics analogy: Quasi-geostrophic theory, *Q. J. R. Meteorol. Soc.*, *120*, 713–731, doi:10.1002/qj.49712051710.
- Bosart, L. F., G. J. Hakim, K. R. Tyle, M. A. Bedrick, W. E. Bracken, M. J. Dickinson, and D. M. Schultz (1996), Large-scale antecedent conditions associated with the 12–14 March 1993 cyclone (“Superstorm ‘93”) over eastern North America, *Mon. Weather Rev.*, *124*, 1865–1891, doi:10.1175/1520-0493(1996)124<1865:LSACAW>2.0.CO;2.
- Čampa, J., and H. Wernli (2012), A PV perspective on the vertical structure of mature midlatitude cyclones in the Northern Hemisphere, *J. Atmos. Sci.*, *69*, 725–740, doi:10.1175/JAS-D-11-050.1.
- Cavallo, S. M., and G. J. Hakim (2009), Potential vorticity diagnosis of a tropopause polar cyclone, *Mon. Weather Rev.*, *137*, 1358–1371, doi:10.1175/2008MWR2670.1.
- Cavallo, S. M., and G. J. Hakim (2010), Composite structure of tropopause polar cyclones, *Mon. Weather Rev.*, *138*, 3840–3857, doi:10.1175/2010MWR3371.1.
- Cavallo, S. M., and G. J. Hakim (2012), Radiative impact on tropopause polar vortices over the Arctic, *Mon. Weather Rev.*, *140*, 1683–1702, doi:10.1175/MWR-D-11-00182.1.
- Cohen, J., et al. (2014), Recent Arctic amplification and extreme midlatitude weather, *Nat. Geosci.*, *7*, 627–637, doi:10.1038/ngeo2234.
- Davis, C. A., and K. A. Emanuel (1991), Potential vorticity diagnostics of cyclogenesis, *Mon. Weather Rev.*, *119*, 1929–1953, doi:10.1175/1520-0493(1991)119<1929:PVD0C>2.0.CO;2.
- Dee, D. P., et al. (2011), The ERA-interim reanalysis: Configuration and performance of the data assimilation system, *Q. J. R. Meteorol. Soc.*, *137*, 553–597, doi:10.1002/qj.828.
- Enomoto T., A. Kuwano-Yoshida, N. Komori, W. Ohfuchi (2008), Description of AFES2: Improvements for high-resolution and coupled simulations, in *High Resolution Numerical Modelling of the Atmosphere and Ocean*, edited by K. Hamilton and W. Ohfuchi, chap. 5, pp. 77–97, Springer, New York.
- Enomoto, T., T. Miyoshi, Q. Moteki, J. Inoue, M. Hattori, A. Kuwano-Yoshida, N. Komori, and S. Yamane (2013), Observing-system research and ensemble data assimilation at JAMSTEC, in *Data Assimilation for Atmospheric, Oceanic and Hydrologic Applications (Vol. II)*, edited by S. K. Park and L. Xu, chap. 21, pp. 509–526, Springer, Berlin.
- Honda, M., J. Inoue, and S. Yamane (2009), Influence of low Arctic sea-ice minima on anomalously cold Eurasian winters, *Geophys. Res. Lett.*, *36*, L08707, doi:10.1029/2008GL037079.
- Hoskins, B. J. (1991), Towards a PV- θ view of the general circulation, *Tellus*, *43A*, 27–35, doi:10.1034/j.1600-0870.1991.t013-00005.x.
- Hoskins, B. J., and I. N. James (2014), *Fluid Dynamics of the Midlatitude Atmosphere*, Advancing Weather and Climate Science Series, John Wiley, West Sussex, U. K.
- Hoskins, B. J., M. E. McIntyre, and A. W. Robertson (1985), On the use and significance of isentropic potential vorticity maps, *Q. J. R. Meteorol. Soc.*, *111*, 877–946, doi:10.1002/qj.49711147002.
- Hunt, B. R., E. J. Kostelich, and I. Szunyogh (2007), Efficient data assimilation for spatiotemporal chaos: A local ensemble transform Kalman filter, *Phys. D*, *230*, 112–126, doi:10.1016/j.physd.2006.11.008.
- Inoue, J., and M. E. Hori (2011), Arctic cyclogenesis at the marginal ice zone: A contributory mechanism for the temperature amplification?, *Geophys. Res. Lett.*, *38*, L12502, doi:10.1029/2011GL047696.
- Inoue, J., T. Enomoto, T. Miyoshi, and S. Yamane (2009), Impact of observations from Arctic drifting buoys on the reanalysis of surface fields, *Geophys. Res. Lett.*, *36*, L08501, doi:10.1029/2009GL037380.
- Inoue, J., M. E. Hori, and K. Takaya (2012), The role of Barents Sea ice in the wintertime cyclone track and emergence of a warm-Arctic cold-Siberian anomaly, *J. Clim.*, *25*, 2561–2568, doi:10.1175/JCLI-D-11-00449.1.
- Inoue, J., T. Enomoto, and M. E. Hori (2013), The impact of radiosonde data over the ice-free Arctic Ocean on the atmospheric circulation in the Northern Hemisphere, *Geophys. Res. Lett.*, *40*, 864–869, doi:10.1002/grl.50207.
- Jung, T., M. A. Kasper, T. Semmler, and S. Serrar (2014), Arctic influence on subseasonal midlatitude prediction, *Geophys. Res. Lett.*, *41*, 3676–3680, doi:10.1002/2014GL059961.
- Khon, V. C., I. I. Mokhov, F. A. Pogarskiy, A. Babanin, K. Dethloff, A. Rinke, and H. Matthes (2014), Wave heights in the 21st century Arctic Ocean simulated with a regional climate model, *Geophys. Res. Lett.*, *41*, 2956–2961, doi:10.1002/2014GL059847.
- König-Langlo, G. (2012), *Upper Air Soundings During POLARSTERN Expedition ARK-XXVII to the Arctic Ocean in 2012*, Alfred Wegener Institute, Helmholtz Center for Polar and Marine Research, Bremerhaven, doi:10.1594/PANGAEA.839535.
- Kuwano-Yoshida, A., T. Enomoto, and W. Ohfuchi (2010), An improved PDF cloud scheme for climate simulations, *Q. J. R. Meteorol. Soc.*, *136*, 1583–1597, doi:10.1002/qj.660.
- Lüpkens, C., T. Vihma, E. Jakobson, G. König-Langlo, and A. Tetzlaff (2010), Meteorological observations from ship cruises during summer to the central Arctic: A comparison with reanalysis data, *Geophys. Res. Lett.*, *37*, L09810, doi:10.1029/2010GL042724.
- Miyoshi, T., and S. Yamane (2007), Local ensemble transform Kalman filtering with an AGCM at a T159/L48 resolution, *Mon. Weather Rev.*, *135*, 3841–3861, doi:10.1175/2007MWR1873.1.
- Mori, M., M. Watanabe, H. Shioyama, J. Inoue, and M. Kimoto (2014), Robust Arctic sea-ice influence on the frequent Eurasian cold winters in past decades, *Nat. Geosci.*, *7*, 869–873, doi:10.1038/ngeo2277.
- Nishij, K., H. Nakamura, and Y. J. Orsolini (2015), Arctic summer storm track in CMIP3/5 climate models, *Clim. Dyn.*, *44*, 1311–1327, doi:10.1007/s00382-014-2229-y.
- Ohfuchi, W., H. Nakamura, M. K. Yoshioka, T. Enomoto, K. Takaya, X. Peng, S. Yamane, T. Nishimura, Y. Kurihara, and K. Ninomiya (2004), 10-km mesh meso-scale resolving simulations of the global atmosphere on the Earth Simulator—Preliminary outcomes of AFES (AGCM for the Earth Simulator), *J. Earth Simul.*, *1*, 8–34.
- Reynolds, R. W., T. M. Smith, C. Liu, D. B. Chelton, K. S. Casey, and M. G. Schlax (2007), Daily high-resolution-blended analyses for sea surface temperature, *J. Clim.*, *20*, 5473–5496, doi:10.1175/2007JCLI1824.1.
- Rinke, A., K. Dethloff, W. Dorn, D. Handorf, and J. C. Moore (2013), Simulated Arctic atmospheric feedbacks associated with late summer sea ice anomalies, *J. Geophys. Res. Atmos.*, *118*, 7698–7714, doi:10.1002/jgrd.50584.

- Sato, K., J. Inoue, and M. Watanabe (2014), Influence of the Gulf Stream on the Barents Sea ice retreat and Eurasian coldness during early winter, *Environ. Res. Lett.*, *9*, 084009, doi:10.1088/1748-9326/9/8/084009.
- Screen, J. A., and I. Simmonds (2013), Exploring links between Arctic amplification and midlatitude weather, *Geophys. Res. Lett.*, *40*, 959–964, doi:10.1002/grl.50174.
- Screen, J. A., I. Simmonds, C. Deser, and R. Tomas (2013), The atmospheric response to three decades of observed Arctic sea ice loss, *J. Clim.*, *26*, 1230–1248, doi:10.1175/JCLI-D-12-00063.1.
- Screen, J. A., C. Deser, I. Simmonds, and R. Tomas (2014), Atmospheric impacts of Arctic sea-ice loss, 1979–2009: Separating forced change from atmospheric internal variability, *Clim. Dyn.*, *43*, 333–344, doi:10.1007/s00382-013-1830-9.
- Serreze, M. C., and A. P. Barrett (2008), The summer cyclone maximum over the central Arctic Ocean, *J. Clim.*, *21*, 1048–1065, doi:10.1175/2007JCLI1810.1.
- Serreze, M. C., A. H. Lynch, and M. P. Clark (2001), The Arctic frontal zone as seen in the NCEP-NCAR reanalysis, *J. Clim.*, *14*, 1550–1567, doi:10.1175/1520-0442(2001)014<1550:TAFZAS>2.0.CO;2.
- Shoji, T., Y. Kanno, T. Iwasaki, and K. Takaya (2014), An isentropic analysis of the temporal evolution of East Asian cold air outbreaks, *J. Clim.*, *27*, 9337–9348, doi:10.1175/JCLI-D-14-00307.1.
- Simmonds, I. (2015), Comparing and contrasting the behaviour of Arctic and Antarctic sea ice over the 35 year period 1979–2013, *Ann. Glaciol.*, *56*, 18–28, doi:10.3189/2015AoG69A909.
- Simmonds, I., and I. Rudeva (2012), The great Arctic cyclone of August 2012, *Geophys. Res. Lett.*, *39*, L23709, doi:10.1029/2012GL054259.
- Simmonds, I., and I. Rudeva (2014), A comparison of tracking methods for extreme cyclones in the Arctic basin, *Tellus*, *66A*, 25252, doi:10.3402/tellusa.v66.25252.
- Simmonds, I., and P. D. Govekar (2014), What are the physical links between Arctic sea ice loss and Eurasian winter climate?, *Environ. Res. Lett.*, *9*, 101003, doi:10.1088/1748-9326/9/10/101003.
- Simmonds, I., C. Burke, and K. Keay (2008), Arctic climate change as manifest in cyclone behavior, *J. Clim.*, *21*, 5777–5796, doi:10.1175/2008JCLI2366.1.
- Takaya, K., and H. Nakamura (2005), Mechanisms of intraseasonal amplification of the cold Siberian high, *J. Atmos. Sci.*, *62*, 4423–4440, doi:10.1175/JAS3629.1.
- Tanaka, H. L., A. Yamagami, and S. Takahashi (2012), The structure and behavior of the arctic cyclone in summer analyzed by the JRA-25/JCDAS data, *Polar Sci.*, *6*, 55–69, doi:10.1016/j.polar.2012.03.001.
- Thompson, D. W. J., and J. M. Wallace (1998), The Arctic Oscillation signature in the wintertime geopotential height and temperature fields, *Geophys. Res. Lett.*, *25*, 1297–1300, doi:10.1029/98GL00950.
- Thompson, D. W. J., and J. M. Wallace (2000), Annular modes in the extratropical circulation. Part I: Month-to-month variability, *J. Clim.*, *13*, 1000–1016, doi:10.1175/1520-0442(2000)013<1000:AMITEC>2.0.CO;2.
- Tilinina, N., S. K. Gulev, and D. H. Bromwich (2014), New view of Arctic cyclone activity from the Arctic system reanalysis, *Geophys. Res. Lett.*, *41*, 1766–1772, doi:10.1002/2013gl058924.
- Vihma, T. (2014), Effects of Arctic sea ice decline on weather and climate: A review, *Surv. Geophys.*, *35*, 1175–1214, doi:10.1007/s10712-014-9284-0.
- Wesslén, C., M. Tjernström, D. H. Bromwich, G. de Boer, A. M. L. Ekman, L.-S. Bai, and S.-H. Wang (2014), The Arctic summer atmosphere: An evaluation of reanalyses using ASCOS data, *Atmos. Chem. Phys.*, *14*, 2605–2624, doi:10.5194/acp-14-2605-2014.
- Zhang, J., R. Lindsay, A. Schweiger, and M. Steele (2013), The impact of an intense summer cyclone on 2012 Arctic sea ice retreat, *Geophys. Res. Lett.*, *40*, 720–726, doi:10.1002/grl.50190.
- Zhang, X., J. E. Walsh, J. Zhang, U. S. Bhatt, and M. Ikeda (2004), Climatology and interannual variability of Arctic cyclone activity: 1948–2002, *J. Clim.*, *17*, 2300–2317, doi:10.1175/1520-0442(2004)017<2300:CAIVOA>2.0.CO;2.